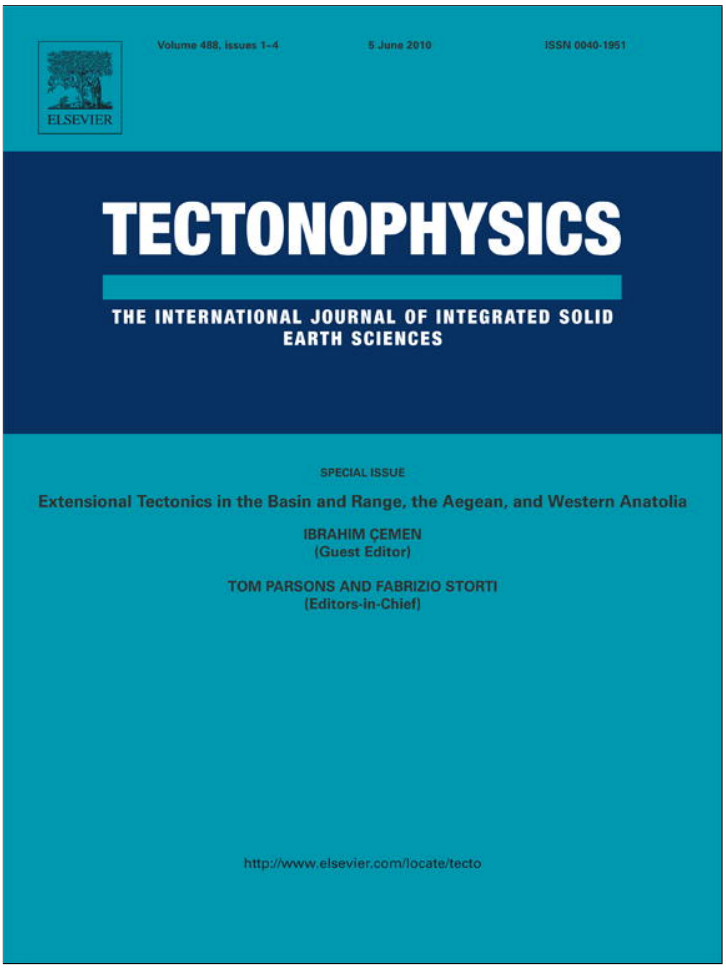

Tectonophysics 488 (2010) 71–86

Contents lists available at ScienceDirect

Tectonophysics

journal homepage: www.elsevier.com/locate/tecto

Faulting in a propagating continental rift: Insight from the late Miocene structural development of the Abert Rim fault, southern Oregon, USA

Kaleb C. Scarberry *, Andrew J. Meigs, Anita L. Grunder

Department of Geosciences, Oregon State University, Corvallis, OR 97331, United States

ARTICLE INFO

Article history:
Received 28 May 2008
Received in revised form 26 July 2009
Accepted 28 September 2009
Available online 9 October 2009

Keywords:
Basin and Range faulting
Basin and Range volcanism
Early Miocene landscape
Oregon geology

ABSTRACT

New geological mapping and ^{40}Ar–^{39}Ar ages reveal a temporal progression of faulting along a major extensional fault (the Abert Rim fault) at the active margin of the Basin and Range Province in the western U.S. The onset of extensional deformation near Lake Abert coincided with widespread basaltic volcanism. Fault cross-cutting relationships and tilt of volcanic layers demonstrate that NW-striking faults formed between ~8.9 and 7.5 Ma and were subsequently cut by the NNE-striking Abert Rim fault. Sequential restoration of cross-sections indicate that the Abert Rim fault south of 42°40′ N latitude had >250 m of stratigraphic separation prior to deposition of the Rattlesnake Tuff at 7 Ma. Low values of net extension (~4%) and long-term rates of geologic deformation (≪1 mm/yr) suggest that regional extension since ~10 Ma has occurred primarily by diking. We model province wide along- and across-strike expansion within the margin of the Basin and Range Province as regional dilation accompanying northward propagation of the Walker Lane transform. The growth of this extensional province is superimposed on a previously unrecognized early Miocene volcanic landscape marked by volcanism between ~21.4 and 22.3 Ma. Dike orientations within one of these early Miocene volcanoes and evidence for the existence of as much as 500 m of paleo-topography prior to widespread deposition of the Steens basalts at ~16 Ma suggests that late Miocene faults near Lake Abert may reactivate an older structural fabric.

1. Introduction

Post-Laramide reorganization of the North American Plate boundary was accompanied by magmatism and the development of the Basin and Range Province in western North America (e.g., Armstrong and Ward, 1991; Wernicke, 1992; Christiansen and Yeats, 1992) (Fig. 1). Deformation at the western margin of the province since ~10 Ma is characterized by east–west extension and right-lateral shear (Zoback, 1989) coupled to the motion of the Pacific Plate, which has moved NNW at a rate of ~52 mm/yr, with respect to North America since ~8 Ma (Atwater and Stock, 1998) (Fig. 1A). Numerous models suggest that forces driving the deformation include: (1) trench pull and subduction zone rollback due to removal of the Farallon slab underneath North America (Humphreys, 1994; Zandt and Humphreys, 2008); (2) rotation of the Cascadia forearc (e.g. Wells and Heller, 1988; Wells et al., 1998); (3) development and propagation of the two principal dextral fault systems of the plate boundary, the San Andreas (Atwater and Stock, 1998) and Walker Lane (Wesnousky, 2005; Faulds et al., 2005); and (4) collapse of the crust driven by gravitational potential energy due to thickening of the Laramide crust (Humphreys and Coblentz, 2007).

Understanding the growth of the northwestern Basin and Range Province (NWBR), which encompasses parts of Oregon, California and Nevada (Fig. 2), in the context of plate boundary and body forces has been limited by the lack of a well-constrained chronological framework for the structural development of the region. In Oregon, faults within the NWBR occur with two principal orientations (NNE-striking and NW-striking) and both cut syn-rift volcanic stratigraphy (Donath, 1962) (Figs. 1B and 2). It is unclear, however, if the two fault sets formed along a pre-Miocene structural fabric (e.g., Donath, 1962; Wells, 1980) or in response to the late Miocene regional stress field (Pezzopane and Weldon, 1993; Crider, 2001). This paper presents results of new $^{40}Ar/^{39}Ar$ ages and detailed geologic mapping within a ~350 km^2 area at the northern end of Lake Abert (Figs. 1B and 3). These data are used to describe the timing and style of faulting within the margin of the NWBR and to place these events in context with Miocene to recent models of the tectonic development of the western margin of North America.

1.1. Regional constraints on Basin and Range extension

Limited data indicate that some extensional faults in the NWBR (Fig. 2; Table 1) formed after 12 Ma (e.g., Colgan et al., 2004), although the temporal and spatial progression are not known in detail. Since the late Oligocene the onset of extensional faulting has migrated westward and northwestward from the interior of the Basin and Range Province in central Nevada (Fig. 1A) into southern Oregon

* Corresponding author. Present address: Geosciences, Colorado State University, 322 Natural Resources Building, Campus Delivery 1482, Fort Collins, CO 80523-1482, United States.
E-mail address: kaleb.scarberry@colostate.edu (K.C. Scarberry).

0040-1951/$ – see front matter © 2009 Elsevier B.V. All rights reserved.
doi:10.1016/j.tecto.2009.09.025

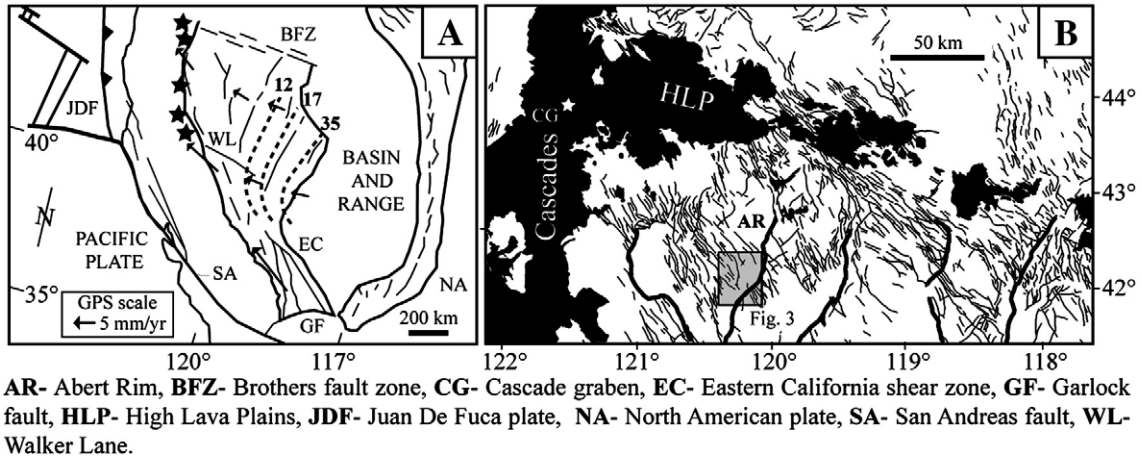

Fig. 1. Tectonic setting of the northwestern Basin and Range Province (NWBR) in the western United States. (A) The seismically active margins of the province are highlighted (after Pezzopane and Weldon, 1993). Stippled lines show progression of onset of extensional faulting (in Ma) (see text). GPS velocity vectors (arrows) from Miller et al. (2001) and Hammond and Thatcher (2005). Cascade volcanoes (black stars) (B) fault map of the northwestern margin of the NWBR highlighting NNE-striking Basin and Range type faults (thick line). Dark shade shows the distribution of Quaternary basalts of the High Cascades and High Lava Plains.

(Fig. 1B) (see summaries by Seedorff, 1991 and Wernicke, 1992; Dilles and Gans, 1995; Miller et al., 1999; Surpless et al., 2002; Colgan et al., 2004; Fosdick and Colgan, 2008). Extension was localized at ~118° W after 26 Ma (Dilles and Gans, 1995) and migrated west to the California-Nevada state line (longitude 120° W) after 14–12 Ma along the Sierra Nevada-Basin and Range transition (Dilles and Gans, 1995; Trexler et al., 2000; Henry and Perkins, 2001; Surpless et al., 2002). Thus, extension migrated westward since the late Oligocene, with more than 100 km of that migration occurring after 15 Ma. Colgan et al. (2008) suggest that the NWBR experienced a two-stage slip history with extensional uplift of ranges occurring between 14–8 Ma and again ca. 4–3 Ma.

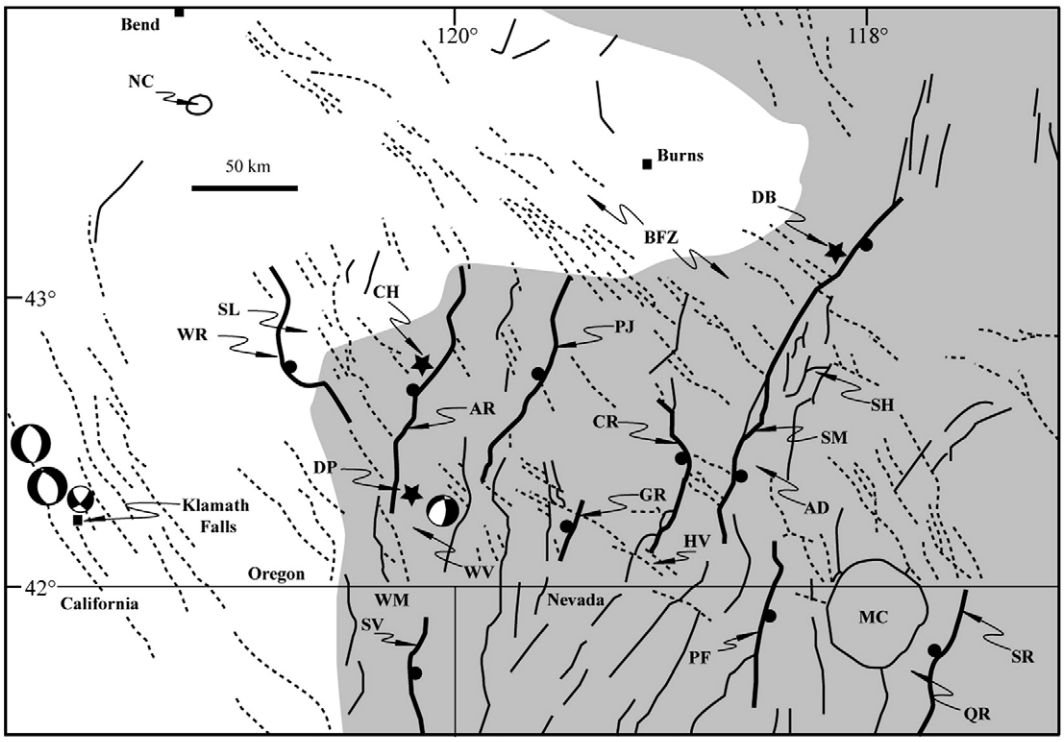

Fig. 2. Major structures of the NWBR after Walker and MacLeod (1991). NNE-striking Basin and Range type faults (solid line), NW-striking faults (stippled line), and eruptive centers discussed in the text (stars). Basin and Range faults discussed in the text (thick solid line) are shown with a ball on the hanging wall block. See Table 1 for information regarding the timing and rate of deformation for individual faults. Fault plane solutions illustrated for two magnitude 6.0 earthquakes near Klamath Falls in 1993 with strike–slip solution highlighted from aftershock sequence (after Crider, 2001). Dual mainshocks of magnitude 5.1 and 5.0, shown by one fault plane solution, occurred within the Warner Valley in 1968 (after Ludwin et al., 1991). Shaded pattern denotes the extent of ~17–15 Ma mafic lavas from Christiansen and Yeats (1992).

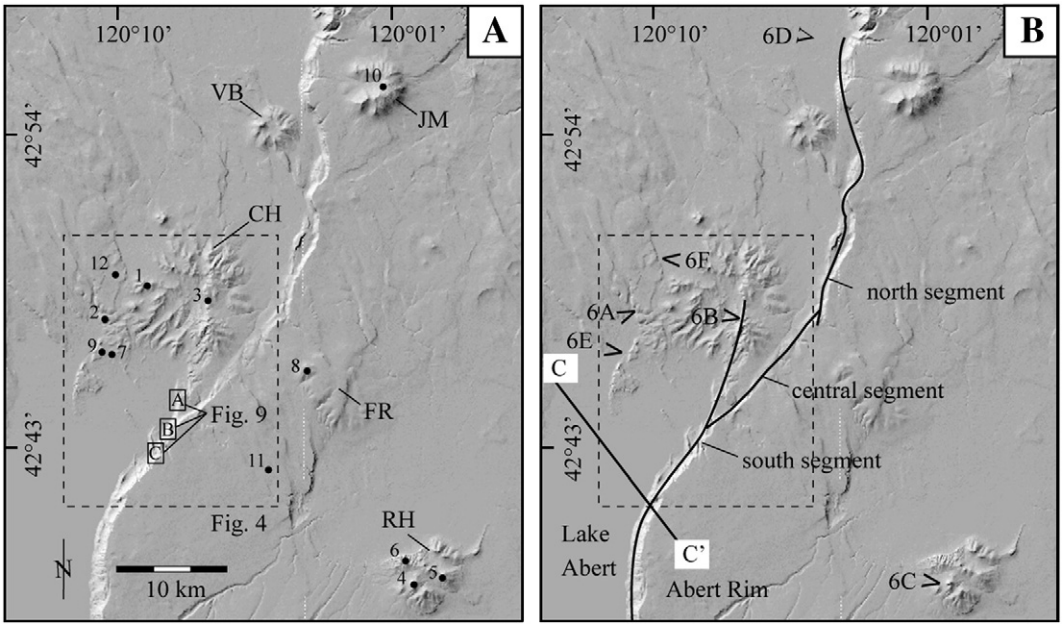

Fig. 3. Digital elevation model of the study region. The Abert Rim fault defines the west margin of the prominent escarpment that extends across the middle of the figure. Dashed box outlines area of detailed mapping shown in Fig. 4. (A) Volcanic features: Juniper Mountain (JM); Venator Buttes (VB); Coleman Hills (CH); Flint Ridge (FR) and Rabbit Hills (RH). See Table 2 for age results of numbered sample locations. (B) The southern, central and northern segments of the Abert Rim fault, as discussed in the text, are marked. Position of Fig. 6 photographs (6A–F) with arrow pointed towards the direction of view. Line of regional cross-section (C–C′, Fig. 12) is shown.

The along-strike, or north–south, growth of the NWBR is less well constrained. The Walker Lane is a dextral shear zone that, along with the San Andreas fault, accommodates transform motion between the Pacific and North American plates (Wesnousky, 2005) (Fig. 1A). Locally, the Walker Lane coincides with the western boundary of the Basin and Range north of 40°N, where it cut the extensional grain of the Basin and Range as it propagated northward between 9 and 3 Ma (e.g., Faulds et al., 2005). To the east, in the Santa Rosa–Pine Forest ranges (Fig. 2; Table 1), extensional deformation after 10 Ma is suggested by footwall cooling ages (Colgan et al., 2004). Extension prior to ~10 Ma is not recorded by thermal, stratigraphic, or structural records (Colgan et al., 2004). These data imply that the locus of extension may have shifted to the NWBR between ~16 and 10 Ma (Christiansen and McKee, 1978; Wernicke, 1992).

Table 1
Timing of initiation and rate of slip for NWBR faults.

Fault system	Lat.[p]	Long.	NNE-strike (rate)	NW-strike
Surprise Valley[a]	41.5 N	120.1 W	14 Ma (~0.4 mm/yr)	na
Santa Rosa range[b]	41.5 N	117.5 W	7.5–10 Ma (0.8 mm/yr)	na
Pine Forest range[b]	41.5 N	118.3 W	8–10 Ma	na
Hawks Valley[c,d]	42.1 N	119.0 W	<10 Ma	~16–10 Ma[q]
Guano Rim[e]	42.2 N	119.5 W	~5 Ma	~9–5 Ma
Drake Peak[f]	42.3 N	120.1 W	>9–7 Ma	16–14 Ma
Steens Mtn. (south)[g,h]	42.5 N	118.5 W	>16.6 Ma	na
Catlow Rim[i]	42.5 N	119.0 W	<16 Ma	na
Sheepshead Mtns.[j]	42.6 N	118.2 W	<7 Ma	12–9 Ma
Poker Jim Rim[k]	42.6 N	119.6 W	<7 Ma	na
Abert rim[k,l]	42.6 N	120.1 W	>6 Ma (0.5 mm/yr)	na
Winter Ridge 42.8 N[i,m]	42.8 N	121.0 W	<6.6 Ma (0.1 mm/yr)[r]	na
Steens Mtn. (north)[n]	43.3 N	118.1 W	~10 Ma	~10 Ma
High Cascade graben[o]	44.1 N	121.6 W	~5 Ma(~1 mm/yr)	na

[a] Colgan et al. (2008).
[b] Colgan et al. (2004).
[c] Maloney (1961).
[d] Legge (1988).
[e] Sawlan et al. (1995).
[f] Wells (1980).
[g] Minor et al. (1987).
[h] Langer (1991).
[i] Walker and MacLeod (1991).
[j] Sherrod et al. (1988).
[k] Hart and Mertzman (1982).
[l] Pezzopane and Weldon (1993).
[m] Jordan et al. (2004).
[n] Johnson and Grunder (2000).
[o] Smith et al. (1987).
[p] See Fig. 2 to locate approximate position of the fault system.
[q] Based on correlation of tuff unit.
[r] Rate calculated here using data from the sources listed.

2. Opening of the Oregon Basin and Range

Net extension within the margin of the NWBR along NNE-striking Basin and Range style faults (Figs. 1B and 2) is thought to be small compared with the central Basin and Range (e.g., Wernicke, 1992). Wells and Heller (1988) estimate ~17 % net extension oriented in a WNW direction perpendicular to a NNW extension direction since ~16 Ma. These results are based primarily on paleomagnetic data and tectonic reconstructions, which require testing against field-based constraint of extension across major regional escarpments such as the Abert Rim fault.

2.1. Major structures

Located within a broad zone of active deformation, the margin of the NWBR is bordered to the west by the Cascade volcanic arc and to the north by the Brothers fault zone (Fig. 1). Topographic and structural relief diminishes northwards towards the Brothers fault zone, a broad NW-striking zone of small en echelon faults that define the northwestern boundary of the Basin and Range (Lawrence, 1976). The High Lava Plains (HLP), a locus of volcanism after ~10 Ma (Walker, 1970; Christiansen and McKee, 1978; Hamilton, 1989; Christiansen et al., 2002) broadly coincides with the Brothers fault zone (Fig. 1B). Thus, the Brothers fault zone appears to function as a transverse zone, an extensional structure associated with magma emplacement (e.g., Rowley, 1998).

Deformation south of the HLP is accommodated by fault systems that exhibit two principal strike directions: NNE and NW (Figs. 1B and 2) (Donath, 1962; Pezzopane and Weldon, 1993; Crider, 2001). NNE-striking faults bound the major topographic escarpments, which are inferred to have the greatest stratigraphic separation. NW-striking faults,

in contrast, exhibit lower topographic and presumably structural relief. A variety of data including analog experiments, dike orientations, cinder cone alignments, slip vectors from earthquake moment tensors, and moderate earthquakes indicate that the fault sets in the region have formed in response to right-oblique extension towards N60–70°W (see summaries in Pezzopane and Weldon, 1993 and Crider, 2001). Geomorphic and paleoseismic observations indicate both fault sets are active (Pezzopane and Weldon, 1993). Field relationships at major escarpments, such as Poker Jim Rim (Mathis, 1993) and Steens Mountain (Hemphill-Haley et al., 1989) (Fig. 2), demonstrate that the two fault sets have mutually cross-cutting relationships, indicating coeval slip at some stage of fault development. Neither the age of initiation nor the duration of motion on either fault set is known regionally.

2.2. Existing constraints on timing of deformation

NNE-striking faults within the margin of the NWBR cut and are thus younger than the ~16 Ma Steens basalt and age-equivalent regional basalts (Fig. 2). The Steens Mountain fault (Fig. 2; Table 1) appears to be a long-lived structure (Minor et al., 1987; Langer, 1991; Hooper et al., 2002). Near the southern end of the fault, an angular unconformity between the Steens basalt and underlying volcanic and volcaniclastic rocks indicates tilting of ~20° prior to 16.6 Ma (Minor et al., 1987; Langer, 1991). Motion on the northern part of the fault coincided with volcanic activity at ~10 Ma (Johnson and Grunder, 2000), and the 9.8 Ma Devine Canyon Tuff is cut and ponded against a NW-striking fault (Johnson, 1995). Well-preserved Holocene scarps at Steens Mountain indicate that the fault remains active (Hemphill-Haley et al., 1989).

West of Steens Mountain, at Poker Jim Rim (Fig. 2; Table 1), there is no angular discordance between Steens basalt and the underlying geologic units (Mathis, 1993) and basalt flows that cap the rim are cut by the range-front fault, which argues that faulting is no older than ~7 Ma (Hart and Mertzman, 1982). A basalt flow banked against the Abert Rim fault (Fig. 2; Table 1) implies the presence of fault-related topography after 16 Ma and before 6 Ma. Faulting along the Abert Rim has been active in the latest Pleistocene (~16 ka), where

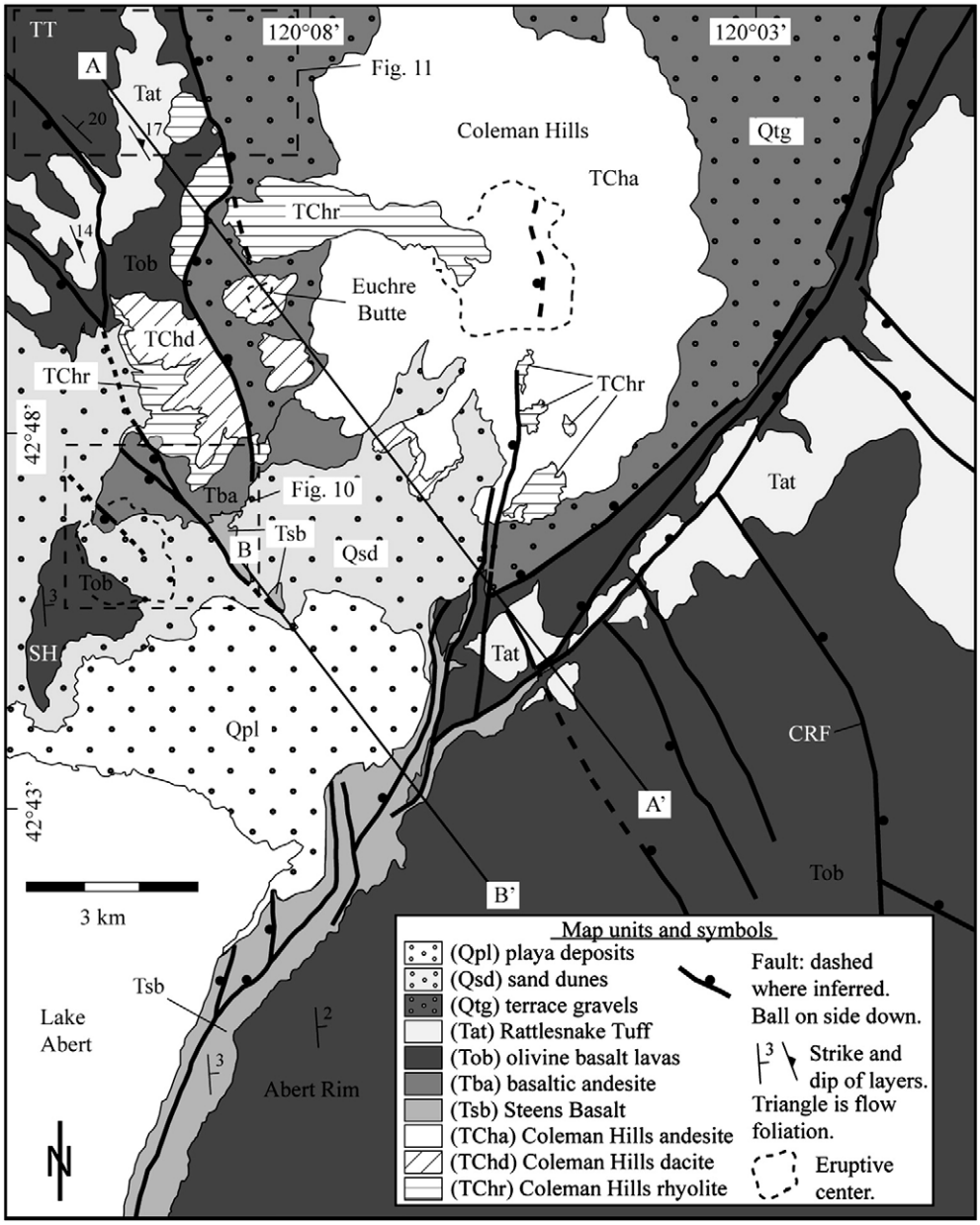

Fig. 4. Sketch geologic map of the northern end of Lake Abert, OR. See Fig. 3 and Table 2 for sample locations, Fig. 5 for lithologic descriptions of geologic units and Fig. 12 for cross-sections (A–A′ and B–B′). Map regions that are discussed in the text or later figures (clockwise from top left): Table Top (TT); Commodore Ridge fault (CRF); and Sawed Horn (SH).

predominately normal slip of offset shoreline deposits implies a ~0.5 mm/yr extension rate (Pezzopane and Weldon, 1993). Mapping at Drake Peak (Fig. 2; Table 1), located near the southern end of the Abert Rim fault, suggests the presence of structural topography on NNE-striking faults prior to 9–7 Ma (Wells, 1980). Therefore the age of extension decreases from south to north along individual NNE-striking faults within the margin of the NWBR.

Although less is known about the age of the NW-striking faults, their activity predates that of the NNE-striking Basin and Range type faults at any particular location across the margin of the NWBR (Fig. 2; Table 1). In the Sheepshead Mountains (Fig. 2; Table 1), a structurally complex region located at the intersection of the HLP with the Steens Mountain fault, NW-striking structures were active between ~12 and 9 Ma prior to post ~7 Ma faulting along NNE-striking structures (Sherrod et al., 1988). A prominent NW-striking graben that formed Hawks Valley (Fig. 2; Table 1), located between Steens Mountain and Guano Rim, developed between ~16–10 Ma within a rhyolite complex (Maloney, 1961; Legge, 1988), which channeled the flow of a younger basalt unit that is cut, in turn, by a NNE-striking fault. At Guano Rim (Fig. 2; Table 1), slight tilting of strata along NW-striking faults occurred between 9 and 5 Ma and preceded faulting along the NNE-striking Guano Rim fault, which has been active since ~5 Ma (ages reported in Sawlan et al., 1995). At Drake Peak (Fig. 2; Table 1) NW-striking faults cut the ~16 Ma Steens basalt but not strata that are younger than ~14 Ma (Wells, 1980).

2.3. The Abert Rim fault

Intersection of NNE-striking and NW-striking faults at the north end of Lake Abert (Fig. 1B) provides an opportunity to evaluate the timing of deformation along the principal fault sets of the NWBR margin. Topographic, and presumably stratigraphic, separation on the Abert Rim fault decline northward, along strike, towards the Brothers fault zone and the High Lava Plains. The geometry of the north end of the Lake Abert basin is controlled by the Coleman Hills and a series of 8–10 faults oriented N30– 40°W (Fig. 3). Langridge et al. (1996) suggest that the association of tufa mounds with a 4300 yr B.P. shoreline of Lake Chewaucan at the northern end of the lake is related to Pleistocene to Holocene fault activity along these NW-striking faults.

3. Methods

Geologic mapping at 1:24,000 scale was conducted over a ~350 km^2 area at the north end of Lake Abert (Figs. 3 and 4). Samples targeted for geochronology were selected to constrain ages of the principal volcanic layers and to provide age brackets for the structurally-related unconformities.

Twelve samples were analyzed using the ^{40}Ar-^{39}Ar technique in labs at the College of Oceanic and Atmospheric Sciences at Oregon State University (Table 2). Samples were prepared as either mineral separates (plagioclase, sanidine, and biotite) or whole-rock cores (~100 mg). Samples and standards (Fish Canyon Tuff biotite, FCT-3, 28.04 Ma) were loaded in quartz tubes and irradiated at the TRIGA reactor facility at Oregon State University. Neutron flux was determined through analysis of the standard. Samples were degassed at 400 °C for 20 minutes prior to sequential analysis over a series of heating steps (experiments) that ranged from 50 to 200 °C in order to optimize instrumental operating parameters. Sequential exposure to Zr-Al getters served to clean the furnace regularly. Analyses were done with a Mass Analyzer Products MAP-215/50 mass spectrometer operating in peak-hopping mode (Duncan and Hogan, 1994; Duncan et al., 1997). Two-σ errors are reported for all analyses.

4. Results

4.1. Geologic mapping and ^{40}Ar–^{39}Ar geochronology

Here we focus on details of the stratigraphic and structural data obtained from the map area (Fig. 4) and provide descriptions and a regional context for additional samples that were collected in the vicinity (Fig. 3). Rocks within the map area form a composite section >400 m thick comprising volcanic rocks in the hanging wall and footwall of the Abert Rim fault (Fig. 5). Early Miocene, dominantly intermediate composition rocks of the Coleman Hills are nonconformably overlain by middle to late Miocene, bimodal, basalt–rhyolite, lava flows and ash-flow tuffs, including the 7.05-Ma Rattlesnake Tuff (Streck and Grunder, 1995). A diverse suite of Pliocene (?) to Quaternary surficial deposits mark the top of the stratigraphic section. Footwall units include the regionally extensive middle Miocene Steens basalt (16.6 –15.3 Ma; Hooper et al., 2002) that crops out at the base of the Abert Rim fault and is disconformably overlain by olivine basalt flows and the Rattlesnake Tuff.

4.2. Geochronology of early Miocene rock units

The oldest units within the study area are early Miocene intermediate to silicic volcanic and intrusive rocks that form the Coleman Hills and Rabbit Hills volcanic complexes (Fig. 3A). These rocks are among the oldest exposures found across southeastern Oregon. Both complexes consist of dominantly intermediate composition lava flows (Walker, 1963; Walker and MacLeod, 1991), but the Coleman Hills have nearly twice the footprint. Fiebelkorn et al. (1983) report a K-Ar age of 29.3 ± 5 Ma for a rock of unknown composition from the Rabbit Hills. This is the only age that has been previously reported for either of these volcanoes. Field relationships within the Coleman Hills demonstrate that rhyolite volcanism preceded eruption and intrusion of dacite and basaltic andesite (Fig. 5), despite the fact that ages for the three lithologies overlap within analytical uncertainty (Table 2). The opposite relationship is observed at the Rabbit Hills, where rhyolite intrudes a section of basaltic andesite lavas.

Table 2
Summary of ^{40}Ar–^{39}Ar age results.

Sample*	Lat.	Long.	Location/type	Mat. dated	Analysis	Steps	%^{39}Ar	K/Ca	Age** (Ma)	2-σ
[1]KCS-04-10	42.8108	120.1394	CH—rhyolite	Sanidine	Plateau	10	100.00	4.485	21.79	0.66
[2]KCS-04-02	42.7869	120.1750	CH—dacite	Plagiolase	Plateau	7	88.69	0.109	21.70	0.56
[3]KCS-04-21	42.7931	120.0847	CH—andesite	Plagioclase	Plateau	8	86.06	0.129	22.02	0.54
[4]KCS-06-24	42.6190	119.9096	RH—rhyolite	Biotite	Plateau	10	93.32	21.561	22.33	0.24
[5]KCS-06-25	42.6170	119.9152	RH—basaltic and.	Plagioclase	Plateau	9	95.03	0.048	23.12	0.48
[6]KCS-06-29	42.6288	119.8999	RH—rhyolite	Whole-rock	Plateau	7	87.79	4.345	20.34	0.36
[7]KCS-05-20	42.7733	120.1714	LA–Steens basalt	Plagioclase	Plateau	8	79.98	0.026	16.12	0.30
[8]KCS-06-16	42.7546	119.9838	FR—dacite	Plagioclase	Plateau	6	81.42	0.117	8.79	0.30
[9]KCS-05-21	42.7731	120.1761	LA—basaltic and.	Plagioclase	Plateau	4	71.51	0.022	8.69	0.42
[10]KCS-06-37	42.9326	119.9272	JM—rhyolite	Biolite	Plateau	10	95.95	20.076	8.58	0.16
[11]KCS-04-43	42.6764	120.0125	LA—basalt	Whole-rock	Plateau	6	83.22	0.042	7.72	0.46
[12]KCS-04-17	42.7933	120.1967	LA—basalt	Whole-rock	Plateau	5	66.95	0.030	7.71	0.42

CH—Coleman Hills, RH—Rabbit Hills, LA—Lake Abert, FR—Flint Ridge, and JM—Juniper Mountain.
*Numbers correspond to sample locations illustrated on Fig. 3. **Plateau ages reported with 2-σ errors.

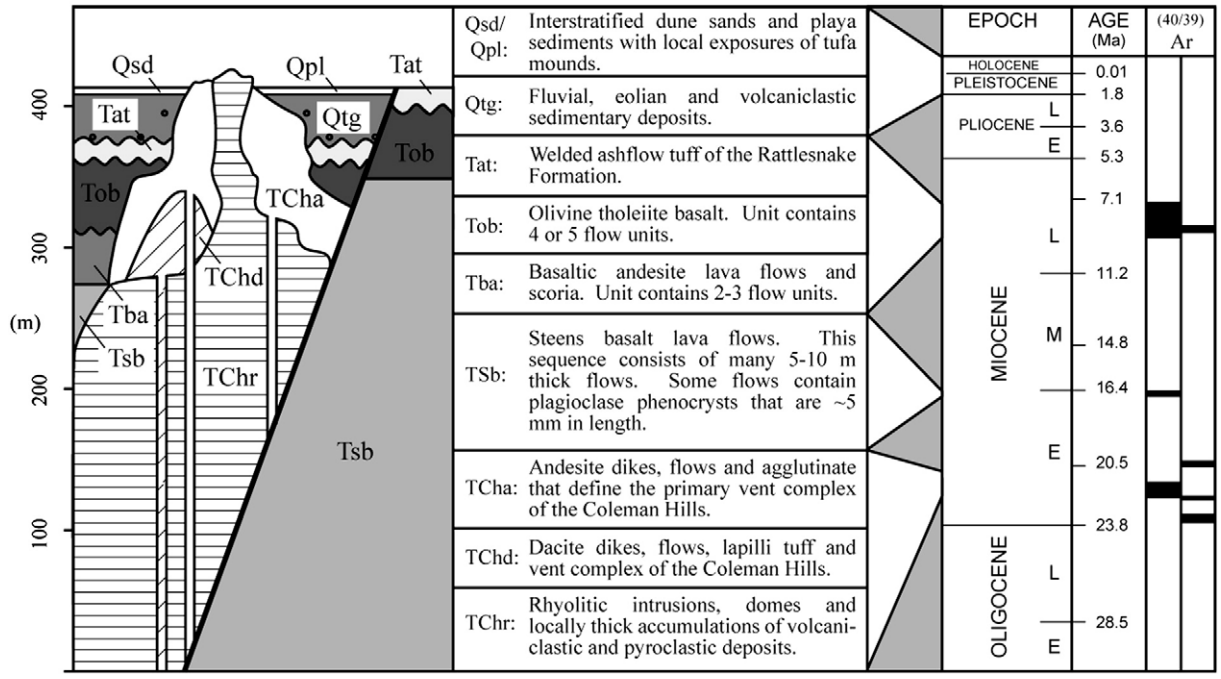

Fig. 5. Stratigraphic column of the map region shows unit thickness and contact relationships within the hanging wall and footwall blocks of the Abert Rim fault. Wavy line represents unconformable contacts between adjacent units. ^{40}Ar–^{39}Ar age data (with errors) are shown on the far right of the diagram.

4.3. The Coleman Hills volcanic suite

Rhyolite volcanism represents the initial phase of magmatism within the Coleman Hills volcanic complex. Intrusion of rhyolite domes was accompanied by explosive eruption, as evidenced by localized rhyolitic surge and block and ash deposits preserved around the margins of the volcano (Fig. 6A). Rhyolite pyroclastic deposits are undifferentiated from rhyolite intrusions on the map (Fig. 4), and the thickness of localized exposures ranges from 3–5 m for block and ash flows and >20 m for surge deposits. The main rhyolite stock is E–W elongate and covers an area of ~10 km^2 in the western part of the complex (Fig. 4). A $^{40}Ar/^{39}Ar$ analysis of a sanidine separate from the stock produced a simple 10-step plateau age of 21.79 ± 0.66 Ma (KCS-04-10; Fig. 7A, Table 2). We use the plateau age rather than the isochron age in all cases.

Dacite of the Coleman Hills is thickest near its source at Euchre Butte (Fig. 4) where a ~50 m section is exposed. Dacite flows, fed by dikes 3–5 m wide, cap a narrow paleochannel filled with a rhyolitic block and ash deposit on the western margin of the Coleman Hills (Fig. 6A). $^{40}Ar/^{39}Ar$ analysis of a plagioclase separate obtained from the top of the dacite flow sequence produced a 7-step plateau age of 21.70 ± 0.56 Ma (KCS-04-02; Fig. 7B, Table 2). The ^{39}Ar release pattern has a small amount of excess argon in the low temperature steps (Fig. 7B), indicative of incomplete equilibration of the magma with the atmosphere.

An extensive scoria tuff and dike swarm defines the main vent and principal volcanic edifice of the Coleman Hills volcano (Fig. 4), which is dominantly andesite and basaltic andesite in composition (Scarberry, 2007). Andesite dikes 3–5 m thick cut dacite units (Fig. 6B) and feed flows that radiate from the center of the volcano. The thickness of this unit ranges from ~75–150 m (Fig. 5). $^{40}Ar/^{39}Ar$ analysis of a plagioclase separate from glass along the margin of a basaltic andesite dike (Fig. 6B) produced an 8-step plateau age of 22.02 ± 0.54 Ma (KCS-04-21; Fig. 7C, Table 2). ^{39}Ar release in this sample shows the effects of ^{39}Ar recoil in the early temperature steps (Fig. 7C).

4.4. The Rabbit Hills volcanic suite

The Rabbit Hills are characterized by a thick sequence of intermediate composition lavas that form the prominent edifice of the volcano. $^{40}Ar/^{39}Ar$ analysis of a plagioclase separate from a basaltic andesite flow near the base of the ~100 m thick lava section produced a 9-step plateau age of 23.12 ± 0.48 Ma (KCS-06-25; Fig. 7D, Table 2). The effects of ^{39}Ar recoil are observed in the early temperature steps (Fig. 7D). Episodes of rhyolite magmatism are recorded by intrusions. $^{40}Ar/^{39}Ar$ analysis of a biotite separate from a massive, crystal-rich rhyolite dome within the center of the volcanic complex (Fig. 6C) produced a 10-step plateau age of 22.33 ± 0.24 Ma (KCS-06-24; Fig. 7E, Table 2), and analysis of a whole-rock core from the devitrified outer margin of a dome complex along the northwestern margin of the volcano produced a 7-step plateau age of 20.34 ± 0.36 Ma (KCS-06-29; Fig. 7F, Table 2). The former sample displays a relatively uniform ^{39}Ar release pattern (Fig. 7E), while the latter shows the effects of ^{39}Ar recoil in the highest temperature steps (Fig. 7F).

4.5. Geochronology of middle to late Miocene rock units

Middle to late Miocene volcanic rocks in the study region (Fig. 3) consist of a bimodal, dominantly mafic, basalt–rhyolite suite that was deposited between ~16 and 7 Ma (Fig. 5). These rocks are similar in age and composition to volcanic deposits that occur within the High Lava Plains (Jordan, 2001; Jordan et al., 2004; Scarberry, 2007).

The Steens basalt crops out within many of the largest fault escarpments of the NWBR margin (Fig. 2) and was deposited between 16.6 and 15.3 Ma (Hooper et al., 2002). Correlation of sections of Steens basalt on the basis of age, chemical and paleomagnetic data suggests that the unit has a maximum thickness of ~450 m within the Abert Rim footwall block (Mankinen et al., 1987). A ~350 m section of Steens basalt exposed in the Abert Rim footwall disappears in the subsurface, from south to north, over an along-strike distance of ~12 km (Fig. 4). Only the top ~30 m of this unit is observed in the Abert Rim hanging wall (Fig. 5). $^{40}Ar/^{39}Ar$ analysis of a plagioclase separate from the top of the hanging wall section produced an 8-step plateau age of 16.12 ± 0.30 Ma (KCS-05-20; Fig. 8A, Table 2). ^{39}Ar release in this sample shows slight effects of ^{39}Ar recoil in the early temperature steps (Fig. 8A).

Silicic units at Flint Ridge and Juniper Mountain (Fig. 3A) were sampled to test their fit with a regional, westward-younging age progression for the initiation of silicic volcanism of the High Lava Plains

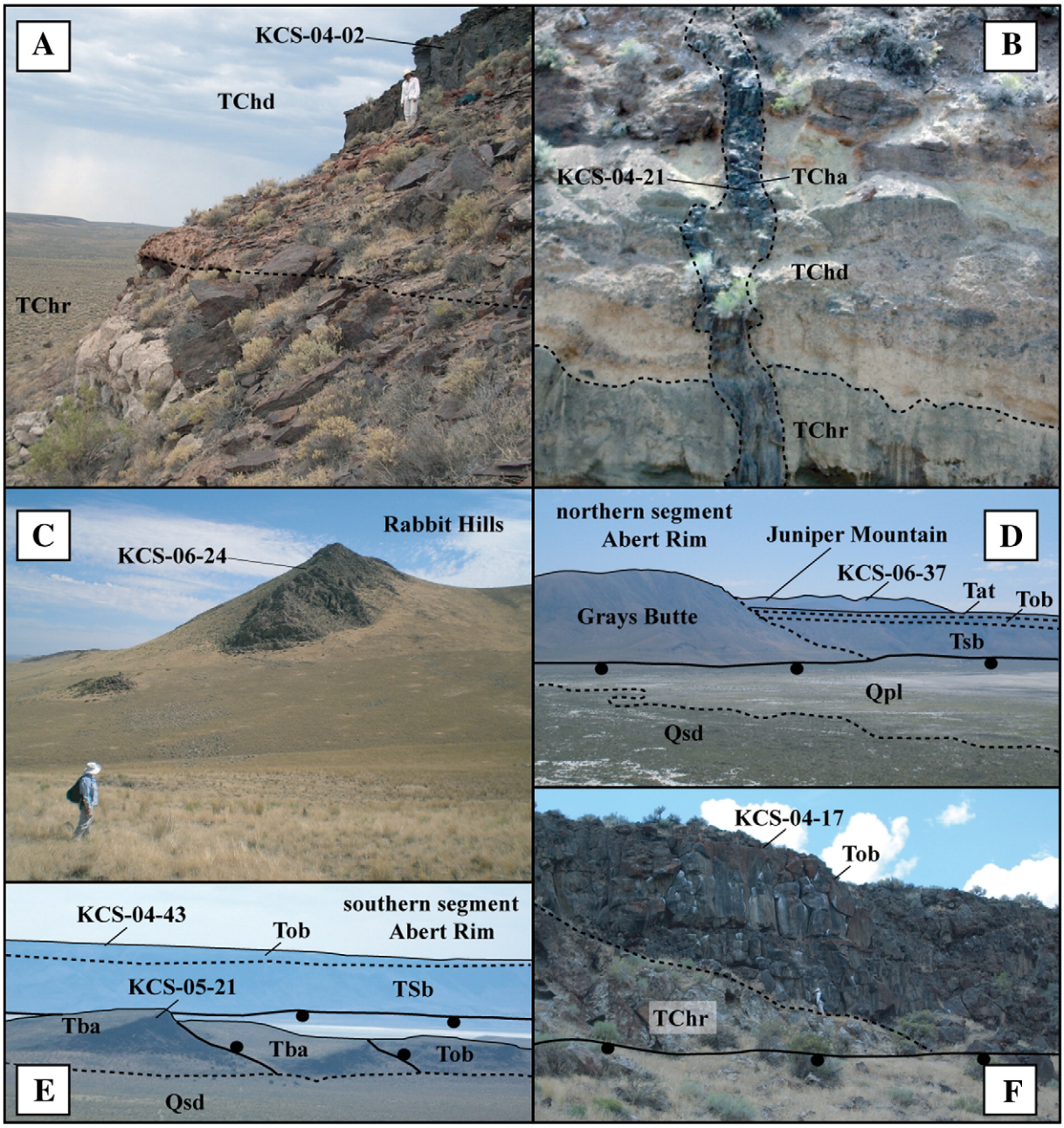

Fig. 6. Photographs illustrate key field relationships and selected sample locations within the study area. Contacts (dashed line) and faults (solid line) are shown with ball on side down. A,B—Exposures that establish the relative age of the principal geologic units of the Coleman Hills volcanic complex (see Fig. 3). C—Rhyolite intrusion within the Rabbit Hills. D—Juniper Mountain in the footwall block of the Abert Rim fault. E—Angular unconformity between Tba and Tob within the hanging wall block of the Abert Rim fault. F—Tob banked onto TChr demonstrates paleotopographic contact between the two units.

(Walker and MacLeod, 1991; Jordan et al., 2004). $^{40}Ar/^{39}Ar$ analysis of a plagioclase separate from the vitrophyre of a dacite flow at Flint Ridge produced a 6-step plateau age of 8.79 ± 0.30 Ma (KCS-06-16; Fig. 8B, Table 2). $^{40}Ar/^{39}Ar$ analysis of a biotite separate from a subcrop of a rhyolite flow obtained from the top of Juniper Mountain (Fig. 6D) produced a 10-step plateau age of 8.58 ± 0.16 Ma (KCS-06-37; Fig. 8C, Table 2). Both ages are in close agreement with the regional trend and suggest that isochrons of age-progressive volcanism of the High Lava Plains extend south into the Basin and Range.

Late Miocene basaltic andesite and basalt flows overlie Steens basalt in the mapped area (Figs. 4 and 5). The base of this section consists of at least 40 m of basaltic andesite (Fig. 5) that has geochemical and radiogenic isotopic characteristics, such as higher SiO_2 and $^{87}Sr/^{86}Sr$ and lower $^{143}Nd/^{144}Nd$ (Scarberry, 2007), consistent with a larger degree of interaction with crustal rocks, relative to the overlying basalts. The basaltic andesite sequence consists of 2–3 flows that are exposed only in the Abert Rim hanging wall (Fig. 6E), southwest of the Coleman Hills (Fig. 3). $^{40}Ar/^{39}Ar$ analysis of a plagioclase separate from the top flow produced a 4-step plateau age of 8.69 ± 0.42 Ma (KCS-05-21; Fig. 8D, Table 2). This sample exhibits an excess argon release pattern (Fig. 8D), particularly in the high temperature heating steps. Although there are only four contiguous steps to define the plateau, it includes ~72% of the ^{39}Ar and agrees well with the isochron age of 8.62 ± 0.54 Ma.

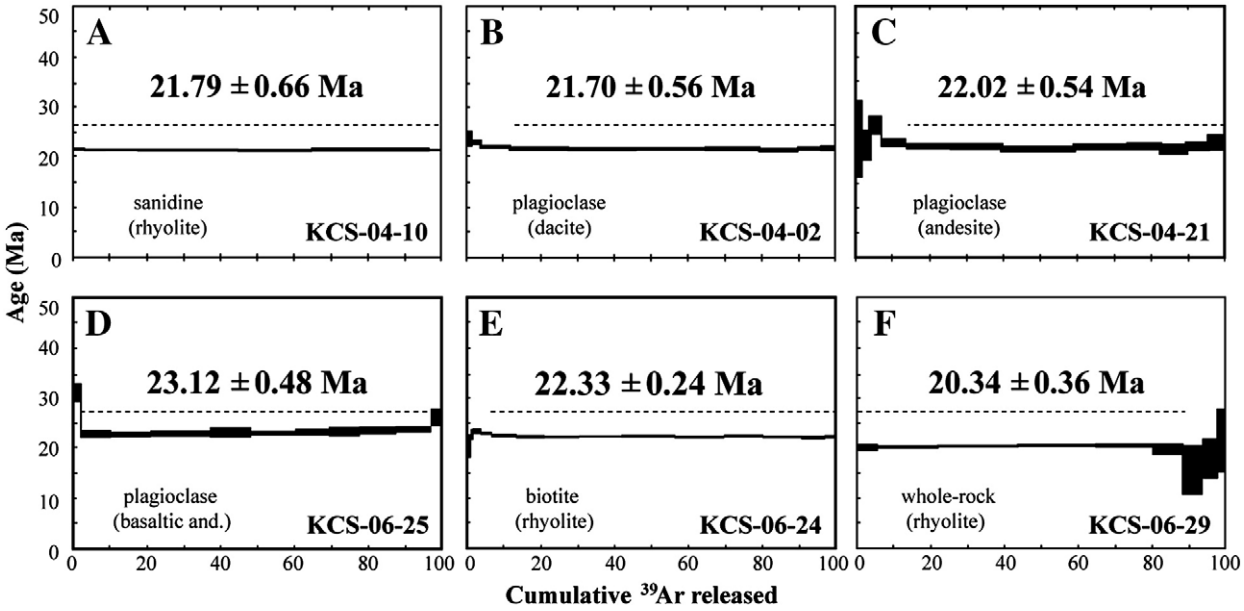

Fig. 7. Argon age spectra for early Miocene volcanic rocks of the Coleman Hills (A–C) and the Rabbit Hills (D–F). The dashed line on the each diagram denotes the steps that were used in the age calculations. The width of the bar is uncertainty in age for a given heating step. Also shown are the mineral and rock types for each sample. Additional sample details are provided in Table 2.

The overlying basalt achieves a maximum thickness of 50–60 m (Fig. 5) and is compositionally similar to high-alumina olivine tholeiite (HAOT) described by Hart et al. (1984). The unit is thickest in the southeastern corner of the map area (Fig. 4) where the basalt section consists of 4 flows, each ~10–15 m thick. $^{40}Ar/^{39}Ar$ analyses of whole-rock cores from the top flow of sections exposed on either side of the Abert Rim fault yield a 6-step plateau age of 7.72 ± 0.46 Ma for basalt in the footwall (KCS-04-43; Fig. 8E, Table 2) and a 5-step plateau age of 7.71 ± 0.42 Ma for basalt in the hanging wall (KCS-04-17; Fig. 8F, Table 2). The footwall sample (Fig. 6E) exhibits a U-shaped ^{39}Ar release pattern (Fig. 8E) that reflects excess argon in the early and late heating steps, whereas the hanging wall sample (Fig. 6F) displays a complex ^{39}Ar release pattern (Fig. 8F) that exhibits excess argon in the low temperature steps and the effects of minor ^{39}Ar recoil in the high-temperature steps. The age and the compositonal character of these basalts earmark them as part of a regional pulse of basaltic volcanism extending throughout the High Lava Plains at ~7.5–7.8 Ma (Jordan et al., 2004).

HAOT lavas are capped by 7.05 Ma Rattlesnake Tuff (Streck and Grunder, 1995) across the northern half of the map area, extending to just south of the Coleman Hills on both flanks of the volcanic complex (Figs. 4 and 5). 10–20 m thick exposures of Rattlesnake Tuff near Lake Abert represent the southern outcrop limit of the tuff in the region.

5. Structural geology

We present detailed structural data for faulting, emphasizing the NW-striking faults within the map area and segmentation of the Abert Rim fault (Fig. 3B). The ~NNE-striking Abert Rim fault is the dominant

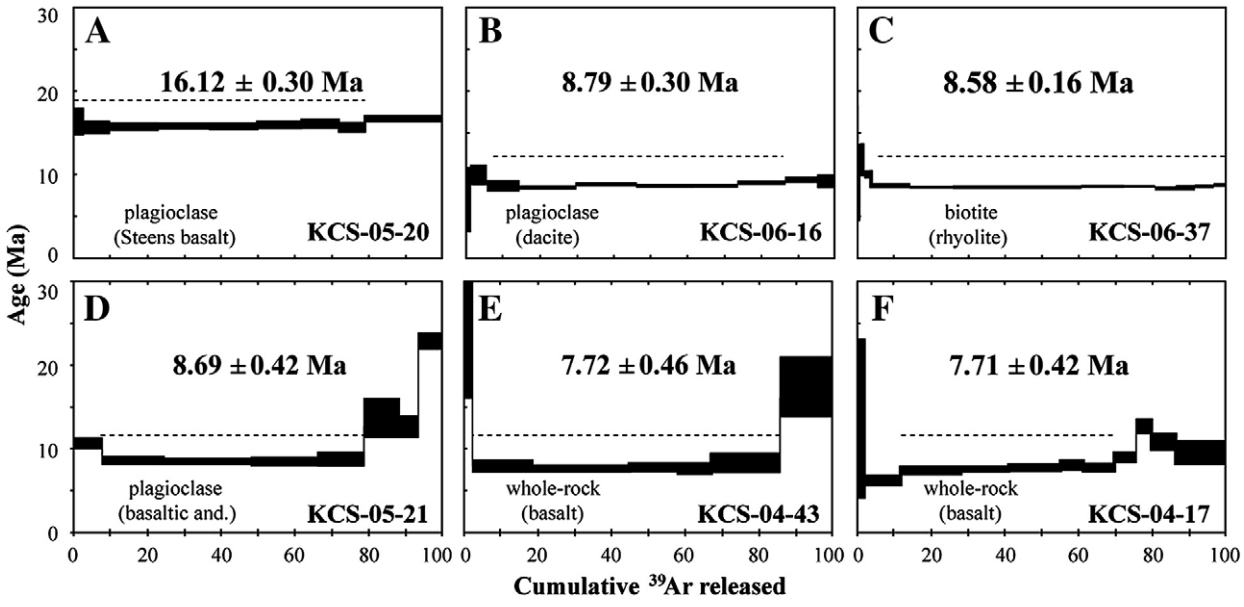

Fig. 8. Argon age spectra for middle and late Miocene volcanic rocks. See Fig. 7 for explanation and Table 2 for additional sample details.

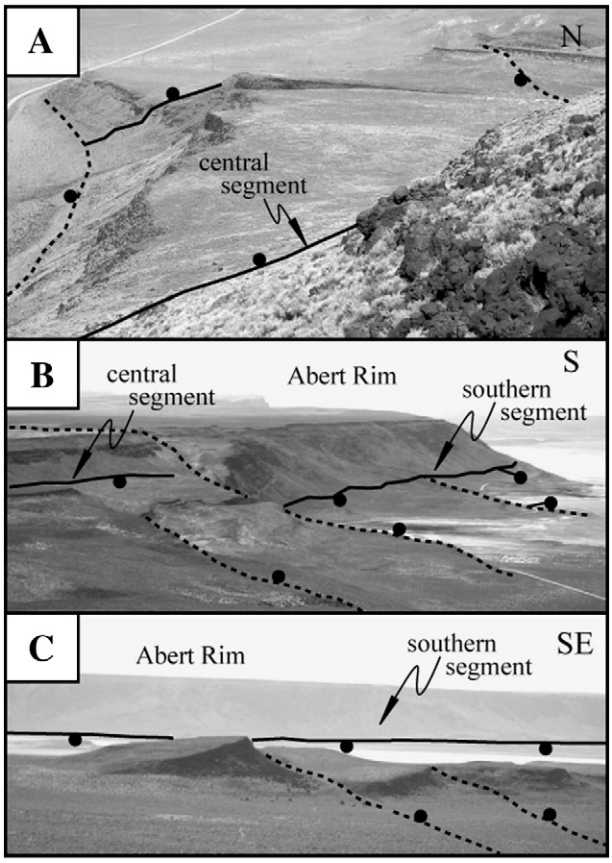

Fig. 9. Photographs illustrate along-strike morphology of the principal NW- and NNE-striking faults, dashed and solid lines, respectively. From south to north along the escarpment (see Fig. 3 for position of photographs): (A) NW-striking faults cut NNE-striking faults, (B) the fault sets are mutually cross-cut, and (C) NNE-striking faults cut NW-striking faults.

structure in the region displaying ~500 m of topographic relief adjacent to Lake Abert (Fig. 3B). NW-striking faults cluster within a ~5–10 km wide zone that is continuous across the Abert Rim fault in the map area (Figs. 4 and 9B).

5.1. Dip of faults

Fault surfaces within the map area (Fig. 4) are not exposed and thus direct measurements from fault planes were not acquired. Measured fault surfaces dip ~50° near Klamath Falls (Gilbert, 1928) (Fig. 2) and ~60° near Steens Mountain (Fuller and Waters, 1929) (Fig. 2). At Summer Lake (Fig. 2), ~35 km NW of the map area, fault planes dip between 60° and 90° (Donath, 1962). The focal mechanism associated with the 1968 seismic event in the Warner Valley (Fig. 2) indicates a high-angle normal fault plane (Ludwin et al., 1991) consistent with observation of nearly vertical slickensides locally within the Warner Valley by Couch and Johnson (1968). On the basis of these observations, and the map expression of the faults near Lake Abert, we assume a uniform fault dip of 70° in our cross-sections (Figs. 10–12 and 14).

5.2. NW-striking faults

The footwall of the Abert Rim fault (Fig. 4) consists of a series of ~2-5°, east-tilted fault blocks that expose middle to late Miocene volcanic layers (Fig. 5). The section is cut by multiple NW-striking faults that have a typical length of ~7 km and an average strike of ~N40°W. These faults produce a series of NW -trending low-relief horst and graben structures. Displacement along any of these faults is difficult to gauge because they cut only Rattlesnake Tuff (Tat) and basalt (Tob), which suggests that they accommodate only modest displacement. The Commodore Ridge fault (Fig. 4) is a ~13 km long, east dipping, ~N-S striking fault that bends NW-ward; it exhibits the most pronounced scarp and offsets the basalt (Tob) by at most ~60 m.

NW-striking faults within the hanging wall of the Abert Rim fault are curved and have more prominent northerly striking segments, relative to NW-striking faults in the footwall block (Fig. 4). These hanging wall

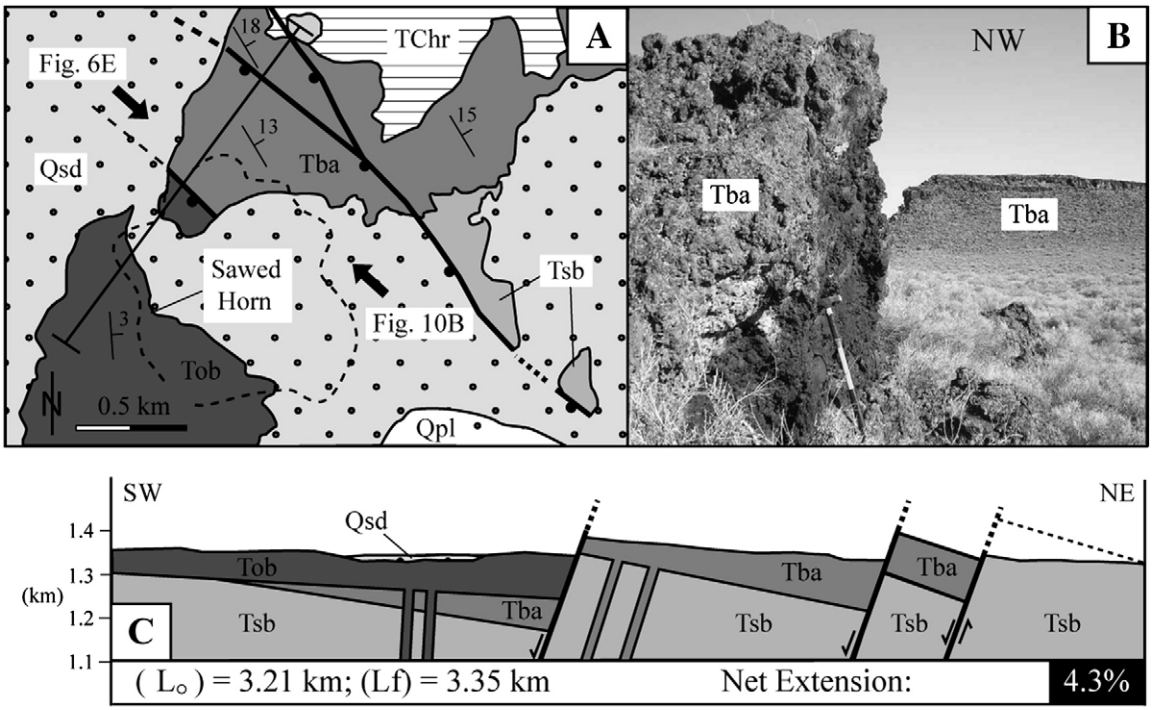

Fig. 10. Relationship between volcanic units and NW-striking faults near Sawed Horn in the western portion of the map region (Fig. 3). A. Map detail highlights the unconformity between older (Tba) and younger (Tob) lavas. Cross-section location shown. See also Fig. 5E for a field photograph. Perspective of photographs illustrated with arrows. B. Scoria and cinders from a sequence of Tba lava flows. C. Cross-section interpretation of unconformable relationships showing the close proximity of NW-striking faults dike systems that feed the lavas.

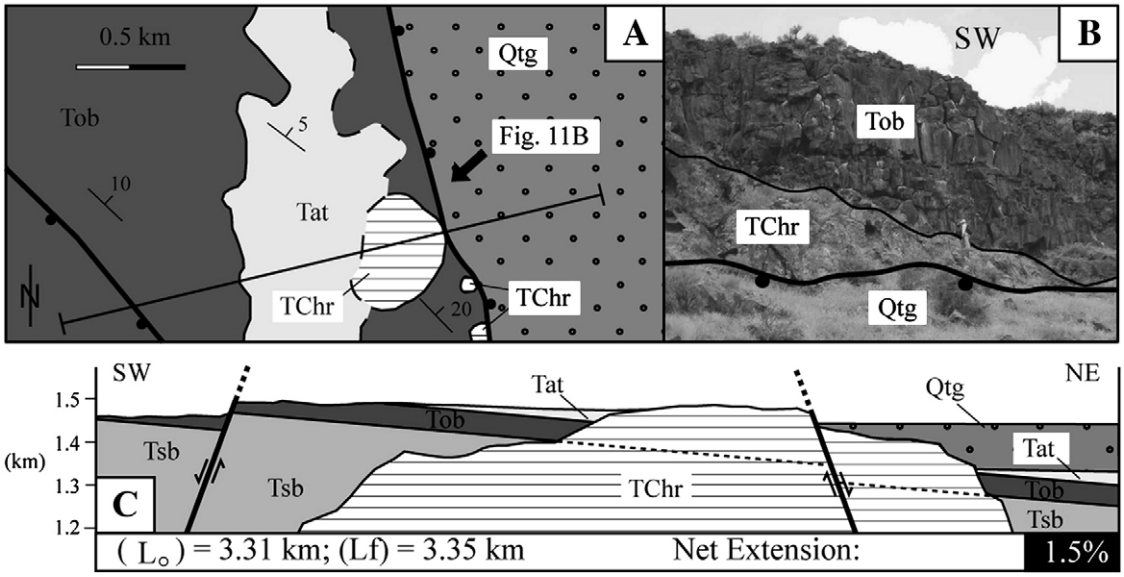

Fig. 11. Relationship between volcanic units and NW-striking faults near Table Top in the northwestern corner of the map region (Fig. 3). A. Map detail highlights onlap of late Miocene volcanic units (Tsb, Tob, and Tat) onto early Miocene rhyolite of the Coleman Hills (TChr). Cross-section location shown. B. Depositional contact between Tob and TChr exposed in a fault scarp. Perspective of photograph illustrated by arrow on panel A. C. Cross-section interpretation showing an angular unconformity between the olivine basalt (Tob) and the Rattlesnake Tuff (Tat).

faults are more complex because they cut rock layers that record differential tilt as a function of age (Figs. 10 and 11). A set of two west-dipping faults located north of the Sawed Horn (Fig. 4) strike ~N40°W. Basaltic andesite (Tba) flows at the base of the sequence dip more steeply northeast than basalt (Tob) in the higher part of the section, which is reflected by a ~10–15° angular unconformity between the 8.6 Ma (Tba) and 7.7 Ma (Tob) units (Fig. 10C). The larger of these two faults can be traced for ~3 km where it splays and bends to the north. Northeast of this zone a ~N15°W trending, east-dipping, ~3 km long fault cuts dacite of the Coleman Hills before bending into a zone that strikes ~N25°E (Fig. 4). To the north, this fault intersects an east-dipping fault that trends ~N15°W and together they form the western margin of a ~N-S-trending basin in which middle to late Miocene volcanic layers are buried by surficial deposits. The northern end of this fault system,

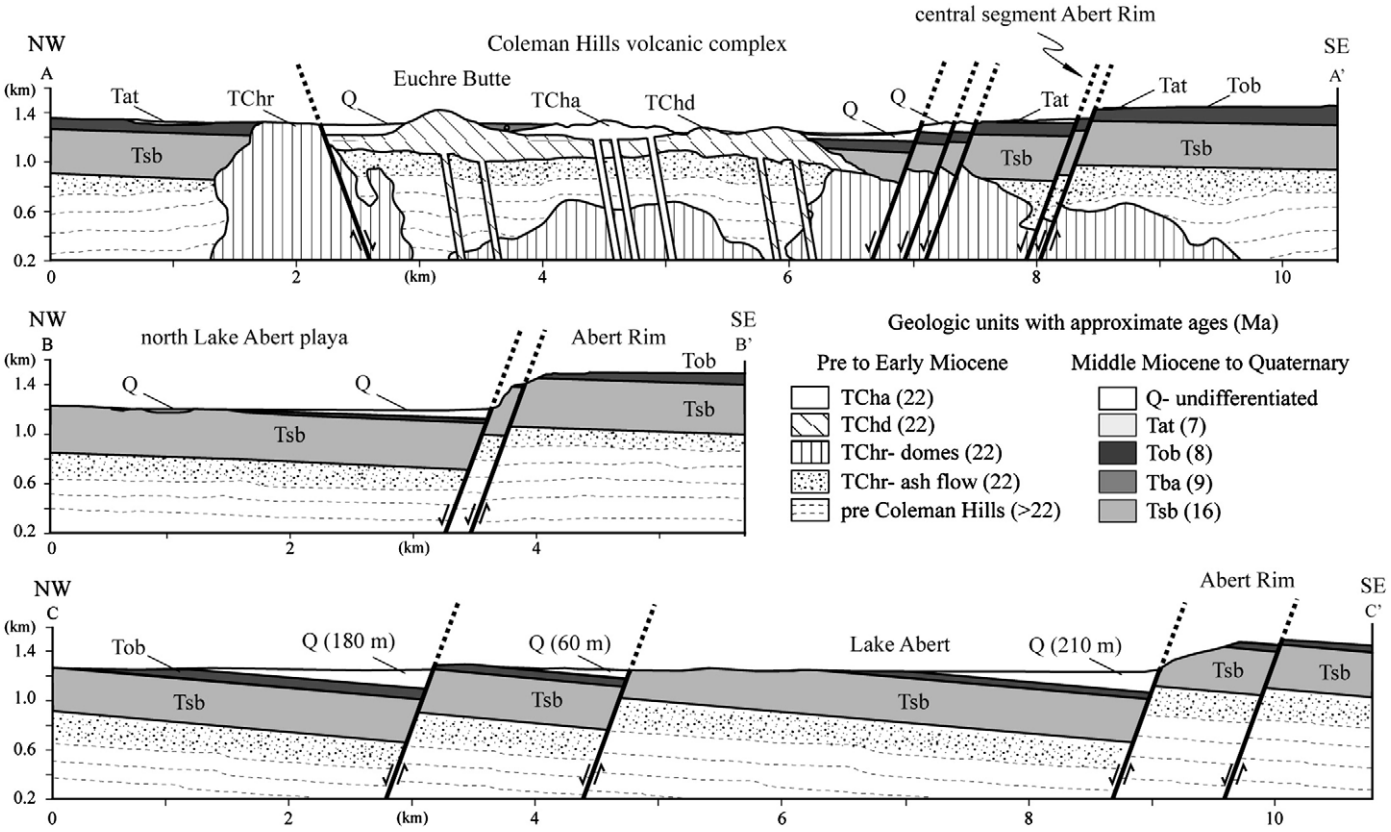

Fig. 12. Cross-sections through the Abert Rim fault and the Coleman Hills. Line of map sections A–A′ and B–B′ shown on Fig. 4 and line of regional section C–C′ shown on Fig. 3. Horizontal length of sections: (A–A′): 10.75 km; (B–B′): 5.80 km; (C–C′): 11 km. No vertical exaggeration. Dip of strata 2° (A–A′and B–B′), 5° (C–C′). Faults dip 70°.

near Table Top in the northwestern corner of the map area (Fig. 4), is of particular interest because the footwall block preserves a depositional contact between early and late Miocene units, which exhibit differential tilt (Fig. 11). An angular unconformity of ~5° marks the contact between the 7.05 Ma Rattlesnake Tuff (Tat) and the 7.7 Ma basalt (Tob) (Fig. 5). Deposition of 7.7 Ma basalt (Tob) directly on top of early Miocene rhyolite (TChr) (Fig. 11B) is not seen elsewhere in the study area.

5.3. Segmentation of the Abert Rim fault

The Abert Rim fault is divided into a southern, central and northern segment (Fig. 3B) for these main reasons: (1) the overall trend of the Abert Rim fault gradually changes, from south to north, by ~20°, from a strike of ~N15°E (southern segment) to ~N35°E (central segment), where the fault splays into multiple strands near the south end of the Coleman Hills (Fig. 4), and then back to ~N15°E (northern segment), (2) cross-cutting relationships between NNE- and NW-striking fault groups changes systematically along-strike from south to north (Fig. 9), and (3) topographic relief and the exposed thickness of Steens basalt change along-strike, from one segment to the next.

5.4. Southern segment: Abert Rim fault

The southern segment of the Abert Rim fault includes the group of faults that extend from the southern end of the prominent north-trending fault that cuts the Coleman Hills to the southern edge of the map area (Fig. 4) and beyond (Fig. 3B). The southern segment of the fault controls the eastern extent of the Lake Abert basin and cuts surficial deposits overlying the Coleman Hills. West-dipping faults of this segment strike ~N15°–20°E, collectively, and define the Abert Rim topographic escarpment (cross-section B–B′, Fig. 12). In detail, the fault zone is complex and includes ~N15°W and more easterly striking segments. Short segment lengths characterize the ~N–S trending faults (~1 to 3 km), although the fault that defines the boundary between the central and south segments extends 6–9 km northward into the Coleman Hills. The southern segment extends ~40 km south of the map area where it blends with the Warner Mountains near Drake Peak (Fig. 2).

5.5. Central segment: Abert Rim fault

Faults of the central segment of the Abert Rim fault strike more easterly (~N35°E), relative to the southern segment. Relatively low topographic relief characterizes the central segment of the fault system (cross-section A–A′, Fig. 12). Topographic relief declines from ~400 m to <200 m between the south and central segments, respectively (Fig. 9B; cross-sections A–A′ and B–B′, Fig. 12) over an along-strike distance of ~3 km (Fig. 4). The decline in topographic relief likely reflects a decline in stratigraphic separation, which is supported by the fact that ~350 m of the Steens basalt is exposed within the southern segment, an outcrop belt that tapers to zero along strike within the central segment of the fault (Fig. 4).

5.6. Northern segment: Abert Rim fault

The northern segment of the Abert Rim fault strikes ~N15°E and is located entirely outside of the map area (Fig. 3B). The multi-strand expression of the Abert Rim fault in the central segment, east of the Coleman Hills (Fig. 4), transitions along-strike to a single through-going fault at the northern segment, where it splits Venator Butte and Juniper Mountain (Fig. 3B). Topographic relief on the northern segment (Fig. 3B) increases along-strike, from south to north, from ~180 m near the Coleman Hills to ~370 m near Grays Butte (Fig. 6D), where a section of Steens basalt also gains exposed thickness along-strike. Further north the topographic expression of the northern segment dissipates and merges with a dense array of NW-striking faults, typical of the Brothers fault zone, within the High Lava Plains (Figs. 1B and 2).

6. Timing of deformation

Sequential development of extensional faults in the Lake Abert region (Fig. 3) is revealed by the structural and stratigraphic relationships between faults and volcanic units (Figs. 4, 5, 10 and 11). From these field relationships and the age data (Fig. 3A; Table 2), three discrete stages in the structural development can be delineated. Oligocene to early Miocene rocks crop out north of the NWBR margin in the John Day basin (Christiansen and Yeats, 1992), and within the southern part of the NWBR (e.g., Duffield and McKee, 1986; Colgan et al., 2004) (Fig. 1B). The Coleman Hills and Rabbit Hills provide the intervening link for understanding early Miocene tectonism of the region.

6.1. Early Miocene deformation

Dikes and dome alignments within early Miocene volcanic strata in the field area exhibit similar orientations to the principal fault systems. Andesite and dacite dikes (Fig. 6B) trend N5°–10°E or N20°–45°W (Fig. 13) and map patterns suggest that rhyolite domes of the Coleman Hills were emplaced along similar trends (Fig. 4). Thus, early Miocene magmatism is associated with a tectonic fabric with the same orientation as both the NW-striking faults and the Abert Rim fault. Onlapping contact relations between the Steens basalt and rhyolite of the Coleman Hills suggests as much as ~500 m of paleorelief existed prior to ~16 Ma (Fig. 11 and cross-section A–A′, Fig. 12). Deposition of the 7.7 Ma basalt (Tob) onto the ~22 Ma Coleman Hills rhyolite (TChr) (Fig. 11) further supports the existence of pre-16 Ma paleorelief. Elsewhere within the NWBR margin, correlated sections of Steens basalt show that the pre-Steens topography was irregular and that local relief of ~1000 m may have existed in places (Wells, 1980; Mankinen et al., 1987). Thus, prior to the middle Miocene Steens basalt volcanism significant topographic relief characterized the landscape of the Lake Abert region.

6.2. Late Cenozoic faulting: 16–7 Ma

Sequential restoration of a cross-section across the southern segment of the Abert Rim fault (Fig. 14) and differences in tilt of late Miocene volcanic layers cut by NW-striking faults (Figs. 10 and 11) indicate that NNE-striking and NW-striking faults were both active in the map region (Figs. 3 and 4) prior to ~7 Ma. A slight angular discordance between the Steens basalt and rim-capping basalts along the southern segment of the Abert Rim fault (Fig. 4), although not easily measured because it is not more than 1–2°, is similar to relationships observed to the south, near Drake Peak (Wells, 1980) (Fig. 2).

Vertical separation of Steens basalt across the southern segment of the Abert Rim fault is 530 m (Fig. 14A). Where the southern and central segments of the fault overlap (Fig. 3B), the base of the Rattlesnake tuff has ~260 m of vertical separation (cross-section A–A′, Fig. 12).

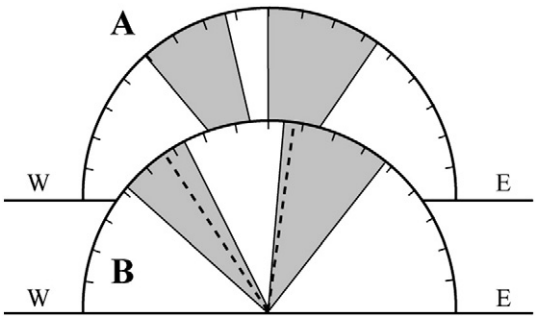

Fig. 13. Comparison of late Miocene fault trends (gray shade) and early Miocene dike orientations (dashed lines). A. Field encompasses the primary trend of NWBR faults that exhibit >100 m offset (after Pezzopane and Weldon, 1993). B. Fault trends and dike orientations within the map region (see Fig. 4).

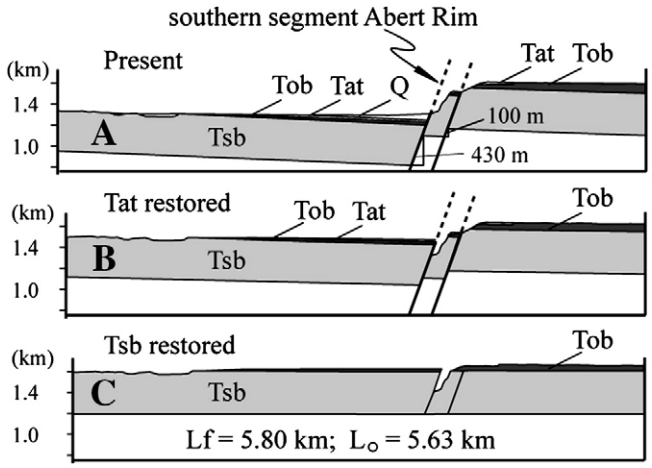

Fig. 14. Restoration of the southern segment of the Abert Rim fault along cross-section line B–B′ (Figs. 4 and 12). A. Present total offset by the fault is ~530 m. B. Restoration of 270 m of vertical offset of Tat leaves 250 m of separation. Tat offset measured from cross-section A–A′ (Fig. 11) and projected south onto cross-section B–B′. C. Restoration of Tsb offset yields net extension of 3% along the fault since ~16 Ma.

Restoring the base of the Rattlesnake tuff reveals that more than half of the present-day structural relief (270 m) existed on the southern segment of the fault prior to deposition of the tuff at ~7 Ma (Fig. 14B). The effect of declining structural relief, from south to north, along-strike of the southern segment of the Abert Rim fault (Fig. 3B) must be considered in the context of this interpretation. As noted, a maximum thickness of ~350 m of the Steens basalt (Tsb) exposed in the escarpment of the southern end of the map region systematically tapers to zero northward over a distance of ~12 km (Fig. 4), therefore losing exposure at a rate of ~30 m/km. Nowhere along this path is Tsb obviously cut by NW-striking faults (Fig. 4). The map distance separating the cross-section lines we use to measure strain (cross-sections A–A′ and B–B′, Fig. 12) is ~3 km (Fig. 4) and therefore a maximum of ~90 m of our interpreted structural relief (Fig. 13B) may be attributed to the effect of decreasing structural relief towards the tip of the fault segment. Thus, at minimum, we estimate that the footwall block of the southern segment had ~180 m of structural relief at ~7 Ma.

NW-striking faults were active in the hanging wall of the Abert Rim fault between 16 and 7 Ma as well. Near the Sawed Horn (Fig. 4), south of the Coleman Hills, 8.6 Ma lavas (Tba) are tilted 10–15° along a pair of west-dipping, NW-striking normal faults and are overlain by 3° northwest dipping 7.7 Ma basalt flows (Tob) (Fig. 10). In the northwestern corner of the map area, near Table Top (Fig. 4), footwall uplift on a west-dipping, NW-striking normal fault between ~7.7 and 7.0 Ma is recorded by a 5° angular discordance between the Rattlesnake Tuff and older basalt (Tob) (Fig. 11).

6.3. Late Cenozoic faulting: post-7 Ma

All volcanic layers younger than 7 Ma are cut by both the NNE-striking and NW-striking faults (Fig. 4) indicating that extension continued along both sets of faults after 7 Ma. Late Pleistocene and Holocene lacustrine, alluvial, and colluvial deposits along the western flank of the Abert Rim escarpment exhibit offset of 4 to 14 m (Pezzopane and Weldon, 1993) and the region as a whole is considered seismically active due to earthquake activity near Klamath Falls in 1993 and the Warner Valley in 1968 (Fig. 2).

7. Magnitude of deformation

Miocene volcanic layers cut by steeply dipping, NNE-striking faults of the Abert Rim fault (Figs. 3 and 4) display small tilts (2°–5°), indicating a small magnitude of extension parallel to the regional NNW–SSE extension direction. Across NW-striking faults, where volcanic layers are tilted as much as 10°–15°, the magnitude of extension is derived by summing extension estimates from individual faults on cross-sections (Figs. 10 and 11). Roughly 100 m of extension (4.3%) occurs across the NW-striking faults in the south near the Abert Rim escarpment (Fig. 10C). Extension diminishes along strike to the north to less than 100 m (1.5%) (Fig. 11C).

Whereas the percent extension across the NNE-striking Abert Rim fault is similar to the NW-striking faults, the magnitude is larger and changes systematically along-strike from south to north. For a 70° fault dip, vertical separation (v) and horizontal extension (h) are 695 m (v) and 490 m (h) in the south (cross-section C–C′; Fig. 12), 530 m (v) and 192 m (h) in the center (cross-section B–B′; Fig. 12), and 270 (v) and 98 (h) in the north (cross-section A–A′; Fig. 12). Assessment of the full width of the Lake Abert basin, assuming an average tilt of 5° and 70° fault dips, yields an estimate of ~490 m of regional extension (4%) (Fig. 12; C–C′).

7.1. Sedimentary basin fill

Structural separation across individual faults is estimated by projecting units at a 5° dip between faults within the Lake Abert basin, which implies that sediment thickness in basins adjacent to faults ranges from 60 m to >200 m above the olivine basalt (Tob) unit (Fig. 12C). This estimate is consistent with other regional estimates obtained from structural studies and seismic surveys. At the north end of Summer Lake (Fig. 2), a thickness of sediment of ~100–300 m was interpreted from seismic refraction data (Donath and Kuo, 1962). A 1–1.5 km thick sediment fill is estimated for the Alvord Desert (Fig. 2) near Steens Mountain (Cleary et al., 1981) and the Quinn River Valley (Fig. 2) adjacent to the Santa Rosa Range (Colgan et al., 2004). These observations show that basins adjacent to NNE-striking faults within the NWBR margin (Figs. 1B and 2) exhibit a systematic decrease in sediment fill, from southeast (1–1.5 km thick) to northwest (300 m thick or less).

8. Geologic rates of deformation

GPS measurement of active deformation across the Basin and Range Province shows that extension decreases systematically with latitude (Fig. 1A) from ~14 mm/yr near 35° N to as little as ~2–7 mm/yr at 42° N (Thatcher et al., 1999; Miller et al., 2001; Bennett et al., 2003; Oldow, 2003; McCaffrey et al., 2007). Published and estimated geologic slip rates range from ~0.1 to 1.0 mm/yr for NWBR faults (Fig. 2), including the High Cascade graben (Fig. 1B), and are presented in Table 1. At Lake Abert a slip rate of ~0.5 mm/yr is calculated for displacement along the southern segment of the fault (Fig. 3B) since ~16 K.y. (Pezzopane and Weldon, 1993). Here we discuss long-term (10^6 years) geologic rates of deformation for faults within the map area (Figs. 3 and 4).

Rates of extension for NW-striking faults are documented at three locations within a 5–10 km wide zone in the study area (Fig. 4): (1) southwest corner of the Abert Rim hanging wall (Fig. 10), (2) northwest corner of the Abert Rim hanging wall (Fig. 11) and, (3) the Commodore Ridge fault (Fig. 4) within the Abert Rim footwall. Individual faults within this zone formed prior to 7.7 Ma and remained active after 7 Ma. An extension rate of 0.3 mm/yr between 8.7 and 7.7 Ma is calculated for a set of three faults located at the southern end of the NW-striking fault system (Fig. 10). Along-strike to the north (Fig. 11), net extension and extension rate decrease. A rate of 0.1 mm/yr is calculated for displacement of Tob during footwall uplift between 7.7 and 7.0 Ma. A rate of ~0.01 mm/yr since 7.7 Ma is calculated for the Commodore Ridge fault within the Abert Rim footwall block. Thus, the greatest rates of extension along NW-striking structures occurred earlier and at a higher rate in the south and subsequently migrated north and deformed at a lower rate with time.

Extension rates for the NNE-striking Abert Rim fault are calculated for southern and central segments of the fault (Figs. 3 and 9B) at time

windows between 7.7 and 7 Ma and after 7 Ma. Extension on the southern segment of the fault occurred at a rate of ~0.4 mm/yr following deposition of the 7.7 Ma basalt (Tob) and prior to eruption of the 7.05 Ma Rattlesnake Tuff (Tat). Extension along the central segment of the fault occurred after eruption of the Rattlesnake Tuff and at a rate of ~0.04 mm/yr.

9. Discussion

9.1. Early Miocene tectonics of the NWBR margin

Active arc volcanism inboard of a subduction zone was an important component of the paleogeography of the western margin of North America at ~22 Ma (e.g., Christiansen and Yeats, 1992). The Coleman Hills (Fig. 3), a dominantly andesitic stratovolcano was likely a component of this arc. Dikes associated with emplacement of the Coleman Hills occurred along a set of conjugate shear fractures (Fig. 13), consistent with a transtensional arc setting (Nakamura and Uyeda, 1980). Eruption of the regionally extensive Steens basalt at ~16 Ma, typically ascribed to the earliest phase of Columbia River Basalt volcanism (e.g., Christiansen and Yeats, 1992), is of debated tectonic significance ranging from impact of a mantle plume to initiation of back-arc spreading (e.g., Hooper et al., 2002; Camp and Ross, 2004).

Basin and Range normal faults in southern Oregon are interpreted to form in response to the modern regional stress field (Pezzopane and Weldon, 1993; Crider, 2001). The occurrence of early Miocene dikes (Fig. 6B) that mimic late Miocene fault trends (Fig. 13) suggests that at least minor early Miocene extensional faulting near Lake Abert accompanied growth of the Coleman Hills volcano prior to middle Miocene Steens volcanism and that faulting after 8.7 Ma may have reactivated a pre-existing regional structural fabric. Several NNE-striking dikes feed mid to late Miocene basalt flows at Drake Peak (Wells, 1980). Thus, observation of faults and dikes associated with the Abert Rim fault support the idea that extensional faulting in the region occurs in response to a redistribution of surface forces acting on a preexisting crustal fracture system (e.g., Donath, 1962; Wells, 1980).

9.2. Kinematics of strain transfer from the Walker Lane

Shear deformation associated with relative motion between the Pacific and North American plates (Fig. 1A) extends northwestward from the Walker Lane into Oregon where it is accommodated by clockwise block rotation, perhaps at a near-continuous rate since ~15 Ma (McCaffrey et al., 2007). Pezzopane and Weldon (1993) and Faulds et al. (2005) note that strike–slip faults diffuse into arrays of ~NNE-striking extensional faults of the NWBR. Indeed, strike-slip faulting is observed as far north as Klamath Falls, OR (Fig. 2) where shear deformation terminates along-strike, to the northwest, into extensional faults that bound the modern Cascade volcanic arc (Fig. 1B) (Smith et al., 1987; Sherrod and Smith, 2000). Therefore, we interpret the High Cascade graben (Fig. 2) to reflect the western-most extensional fault system related with the northern limit of Walker Lane shear.

In this framework, we propose a model that reconciles the spatial and temporal progression of extension within the NWBR since ~10 Ma (Fig. 15; Table 1). Extension migrated westward from the Steens fault by 10 Ma, to the Abert Rim fault after 8.7 Ma, to the modern Cascade arc by ~5 Ma. Northward migration of faulting (Fig. 15; Table 1) occurred at ~120°W from the Warner Mountains and Drake Peak region by ~10 Ma (Fig. 2; Table 1) to the southern segment of the Abert Rim fault before 7 Ma (Figs. 9B and 14), to the northern segment of Abert Rim fault, which cuts regional ignimbrite (Tat, Fig. 6D), after 7 Ma. We attribute this pattern of deformation to northwestward propagation of shear at the tip of the Walker Lane system after ~9 Ma (Faulds et al., 2005). In this context, faults of the NWBR are collectively a large-scale example of a "horsetail fan" structure (e.g., Brace and Bombalakis, 1963) where the principal NNE-striking faults (Fig. 2; Table 1) are representative of tensile cracks formed at the edge of a propagating shear crack (Fig. 15).

9.2. Coupled development of NW- and NNE-striking faults

Regional studies show that NW-striking faults formed prior to, or coeval with, the development of NNE-striking faults in any particular area of the margin of the NWBR (Figs. 2 and 15; Table 1). At Lake Abert,

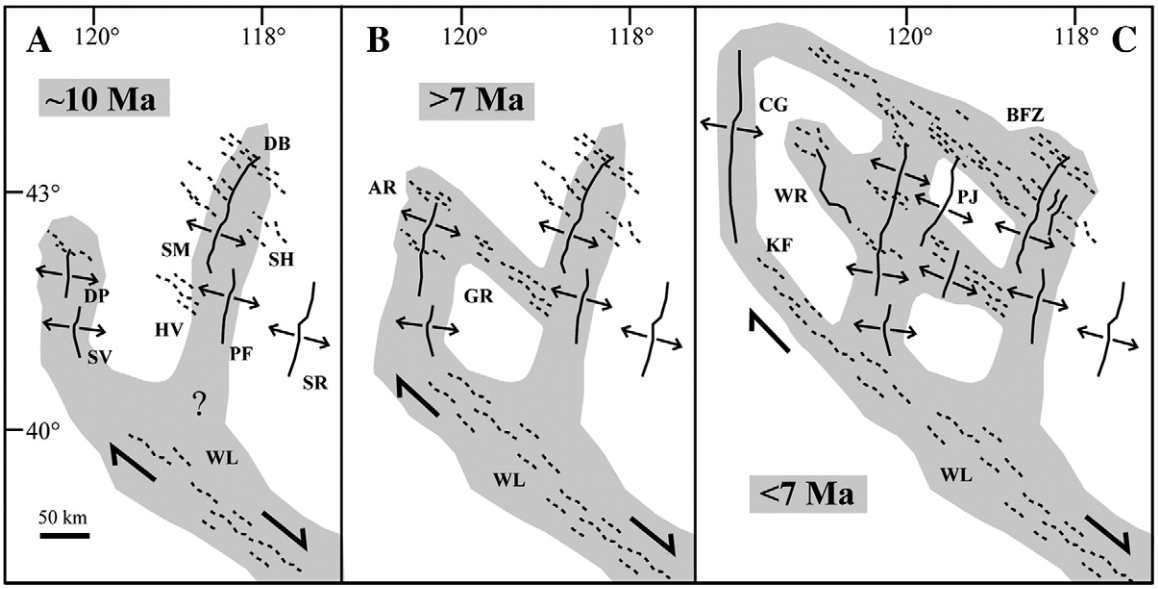

Fig. 15. Regional model for the development of NW- and NNE-striking faults within the northwestern Basin and Range province. See Table 1 for details of the data shown in the figure. Shade pattern highlights zones of deformation. The key features of the model are: (1) the formation of NW-striking faults at the tips of NNE-striking faults and (2) north and westward progression of the development of both fault trends with time.

NW-striking faults formed within a narrow zone (~5 km) at the latitude of the Coleman Hills (Fig. 3) prior to the appearance of a through-going, NNE-striking Abert Rim fault. After 8.7 Ma and before 7 Ma, NW-striking faults accumulated slip and the southern segment of the Abert Rim fault had formed (Figs. 6E and 16). The NW-striking faults formed at the tip of the northward propagating Abert Rim fault (Fig. 16) as indicated by (1) NW-striking faults that diminish in displacement and in age of faulting to the north, (2) NW- and NNE-striking faults that have mutually cross-cutting relations at the boundary between the southern and central segments of the Abert Rim fault (Figs. 3B and 9B), (3) NW-striking faults that are truncated by the Abert Rim fault in the north, and (4) stratigraphic separation diminishes systematically to the north.

We therefore interpret the NW-striking faults of the margin of the NWBR as dilatational fractures associated with the tips of propagating NNE-striking Basin and Range normal fault systems (Fig. 15). Dilational fracturing ahead of propagating normal faults is described elsewhere within the Basin and Range Province (e.g., Trudgill and Cartwright, 1994; Rowley, 1998; Murphy et al., 2004) and within propagating rift systems of Iceland (e.g. Khodayar and Einarsson, 2002; Tentler and Mazzoli, 2005).

Growth of the Abert Rim fault progressed from south to north (Fig. 16). The southern segment exhibits structural relief prior to 7 Ma (Figs. 14 and 16A) whereas the central and northern segments both cut Tat (Figs. 9B and 6E, respectively) and are younger than 7 Ma. The northern (Fig. 6E) and southern segments (Fig. 6D) of the fault exhibit much greater stratigraphic separation than the central segment (Fig. 9B). Based on these observations we interpret the central segment as a relay-ramp structure (e.g., Trudgill and Cartwright, 1994) that links the tips of the southern and northern segments (e.g., Densmore et al., 2005) of the Abert Rim fault (Fig. 16C).

9.3. Implications for the kinematic nature of the Brothers fault zone

Our model (Fig. 15), in which NW-striking faults are dilational fractures formed and subsequently deactivated as the tip of NNE-striking normal faults propagate northward, provides a new explanation for the termination of the NWBR in general and for the Brothers fault zone (BFZ) in particular. As has been noted since Lawrence (1976) first documented the BFZ, thousands of short, NW-striking, low topographic relief faults make up the fault system and that nowhere is the BFZ expressed as a single through-going fault zone (Fig. 2). What has not been appreciated, however, is that fault density within the BFZ is greatest near the tips of the principal NNE-striking basin-bounding faults (Figs. 1B and 2). If NW-striking faults are structurally (and spatially) linked to the tips of the NNE-striking faults, their alignment in a northwest trending zone (the BFZ) implies that their location reflects the extent of northward propagation of the NNE-striking faults and not a nascent transform boundary comparable to the Garlock fault of southern California.

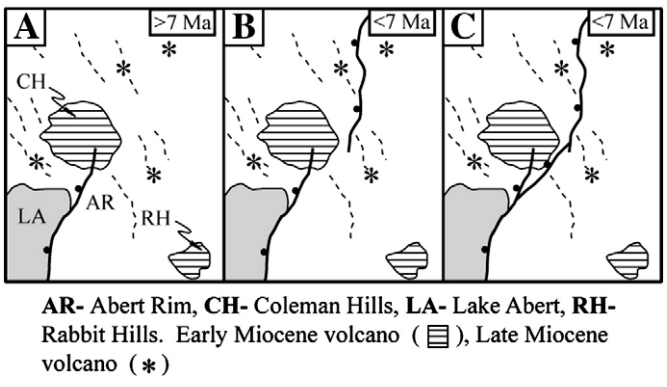

Fig. 16. Model for the segmented growth of the Abert Rim fault during the late Miocene. See Fig. 3 and text for detailed description of the southern, middle, and northern segments of the fault.

9.4. Geologic rates of extension

Long-term (10^6 yrs) rates of extension across the Lake Abert basin are low ($\ll$1 mm/yr) because they document a small component of a larger system. McCaffrey et al. (2007) show that ~9 mm/yr of motion occurs across the entire Basin and Range province as the southern Cascadia forearc moves NW with respect to the Wasatch Mountains in Utah. Geologic and geodetic rates of extension across the whole of southeastern Oregon are ~4–6 mm/yr (Pezzopane and Weldon, 1993) and between 1–4 mm/yr (Thatcher et al., 1999; Hammond and Thatcher, 2005), respectively. If rates across the Lake Abert basin (Fig. 12C) are a proxy for rates across the entire NWBR margin, then we estimate a long-term (10^6 yrs) extension rate on the order of ~1 mm/yr for the Basin and Range province in southeastern Oregon since ~10 Ma.

We propose that magmatic addition through dike injection may compensate for the difference between low rates of extension measured on the cross-sections and implied by the regional topography and the higher rates implied by other data sets. Voluminous basaltic magmatism in both the NWBR margin and in the High Lava Plains reflects the likely occurrence of an extensive dike and fault network in order to link the mantle source with the surface and also mask the presence of that network due to burial beneath successively younger lava flows. In East Africa, magma intrusion is a primary process involved in strain accommodation during the early stages of continental rifting (Calais et al., 2008). Furthermore, magmatism accommodates extension along Basin and Range faults that project into the eastern Snake River Plain (e.g. Rodgers et al., 2002), near the northeastern margin of Basin and Range extension in the western U.S.

Pezzopane and Weldon (1993) measure a Quaternary extension rate of ~0.5 mm/yr for the Abert Rim fault that is an order of magnitude larger than our long-term estimate for the same fault. Although our selection of an average fault dip of ~70° (e.g., Fig. 12) maximizes this difference, as the long-term rate could approach ~0.1 mm/yr with shallower fault dips of 50 to 60°, we believe that the discrepancy more likely reflects changes in the rate of extension during the development of the fault system. At Abert Rim we envision a pulse of extension, and diking, associated with the onset of magmatism (e.g., Fig. 16A) that was followed by a prolonged interval where the extension rate decreased. Other studies suggest that the rate of extension, or strain accommodation, increased both at Abert Rim (Pezzopane and Weldon, 1993) and across the Basin and Range (McCaffrey et al., 2007) sometime during the past few million years.

10. Conclusions

This study provides new insight into the spatial and temporal development of structures and magmatism in the northwestern Basin and Range extensional province. At the scale of the NWBR margin (Fig. 2; Table 1), our analysis reveals that Basin and Range fault initiation within southeastern Oregon systematically progressed from southeast to northwest during the late Miocene. This northward and westward expansion involved faulting on NW-striking faults localized at the tips of northward propagating NNE-striking Basin and Range faults, of which the Abert Rim fault, the focus of this study, is one example (Fig. 16). Dilation of the northwestern Basin and Range Province accommodated the northwestward propagation of the Walker Lane belt from northwestern Nevada towards the Cascade graben system in southern Oregon.

The middle Miocene to Recent structural evolution of the Abert Rim fault is superimposed on a previously unrecognized early Miocene landscape marked by arc-like volcanism. New ^{40}Ar–^{39}Ar ages (Figs. 7 and 8; Table 2) indicate that Miocene volcanic activity near Lake Abert began ~21–23 Ma at the Coleman Hills and Rabbit Hills (Fig. 3) as large

composite volcanoes erupting andesite to basaltic andesite and relatively small volumes of rhyolite and dacite (Fig. 6A and C). Andesite dikes within the Coleman Hills (Fig. 6B) strike NW and NNE (Fig. 13). The early Miocene landscape was buried by at least ~350 m of the Steens basalt (Fig. 11C; cross-section A–A′, Fig. 12) at ~16 Ma (Fig. 2). The earliest phase of extension along the Abert Rim fault was synchronous with the onset of late Miocene volcanism. Unconformities within the volcanic section (Figs. 10 and 11) and vent alignments within a ~10–15 km wide volcanic rift zone located at the tip of the Abert Rim fault demonstrate coincidence of bimodal volcanic eruptions and motion along NW-striking faults after ~9 Ma and before ~7.5 Ma (Fig. 16A). Eruption of dacite and rhyolite dome complexes at Juniper Mountain and Flint Ridge, ~8.6 and ~8.8 Ma, respectively (Fig. 3A), conform to the pattern of age-progressive silicic volcanism of the High Lava Plains (HLP) (Fig. 1B). Eruption of tholeiitic basalt from Venator Butte (Fig. 3A) and Sawed Horn (Fig. 4) at ~8.6 and 7.7 Ma was part of a regional basalt pulse throughout the HLP.

The Abert Rim fault propagated northward via segment linkage after 7 Ma. Volcanic rocks associated with the tip of the southern segment, for example, were cut due to linkage with the northern segment (Fig. 16). At its northern end, the Abert Rim fault merges into the dense array of NW-striking faults comprising the Brothers fault zone (Fig. 2). Concentration of NW-striking Brothers fault zone faults at the end of the Abert Rim fault mirrors the cross cutting relations between NW- and NNE-striking faults to the south. A model where volcanism is localized along NW-striking faults and NW-striking faults form at the tip of NNE-striking faults explains both the faulting and the concentration of Quaternary volcanism of the HLP (Fig. 1B) at the tips of Basin and Range faults in the BFZ (Figs. 1 and 2).

We measure the long-term (10^6years) rate and magnitude of extension across systems of NW- and NNE-striking faults at different time intervals within our study area. The clearest evidence for fault activity during or following early Miocene volcanism occurs near the western edge of the Coleman Hills (Fig. 4) where thickness, contact relations, and partial restorations of cross-sections argue for ~0.5 km of topographic relief prior to eruption of Steens basalt by ~16.2 Ma. Roughly ~0.25 km extension of the Coleman Hills (~2.5% over 10 km) between ~22 and 16 Ma at a rate of ~1.0 mm/yr is implied. Extension on NW striking faults between ~9 and 7 Ma is ~0.15 km extension (~4.3% over 3.4 km; Fig. 10) at ~0.3 mm/yr at the Sawed Horn between 8.7 and 7.7 Ma and is ~0.05 km extension (~1.5% over 3.4 km; Fig. 11) at a rate of ~0.1 mm/yr at the Table Top between ~7.7 and 7.0 Ma. After ~7 Ma we measure ~0.06 km extension by NW-striking faults (<1% over ~1 km; Fig. 4) at a rate of 0.01 mm/yr. Extension across the southern segment of the NNE trending Abert Rim fault system is ~0.10 km between ~7.7 and 7.0 Ma (~1.6% over ~6 km; Fig. 14B) at a rate of 0.4 mm/yr. Post-7 Ma extension across the central segment is ~0.15 km (~3.8% over 4.0 km; cross-section A-A′; Fig. 12) at a rate of 0.04 mm/yr. These new constraints demonstrate that the long-term extension rates (0.01 to ~1.0 mm/yr) and magnitudes (~1.5 to 4.3%) are low, particularly when compared with rates for short and intermediate timescales in the region. This mismatch can be reconciled in two ways: (1) by allowing that widening of the margin of the NWBR since ~10 Ma has been accommodated in substantial part by magmatic addition, specifically via dike injection and (2) allowing for episodic, rather than continuous, deformation since ~10 Ma. In fact, our data do not preclude a two-stage deformational history for the margin of NWBR in Oregon, at ~14–8 Ma and ca. 4–3 Ma, as is proposed for the southern part of the NWBR in California and Nevada (e.g., Henry and Perkins, 2001; Colgan et al., 2008; Fosdick and Colgan, 2008).

Acknowledgments

The authors would like to acknowledge the USGS EdMap program (award # 06HQAG0083) and the National Science Foundation (Continental Dynamics division EAR-0506869; Tectonics division EAR-0610064) for financial support of this research. We thank Tom Wagner, Andy Uhrig, Chris Johnson, Shawn Majors, Mark Ford, Barry Walker, Emelda Zuschlag and a runaway named Jamie for their help out in the field. Thanks are also due to Bob Duncan and John Huard for their help in obtaining and interpreting the age results. Ray Wells and Jim Faulds provided thoughtful and thorough reviews of this manuscript.

References

Armstrong, R.L., Ward, P., 1991. Evolving geographic patterns of Cenozoic magmatism in the North American Cordillera: the temporal and spatial association of magmatism and metamorphic core complexes. Journal of Geophysical Research 96, 13,201–13,224.

Atwater, T., Stock, J., 1998. Pacific-North America plate tectonics of the Neogene southwestern United States—an update. In: Ernst, W.G. (Ed.), International Geological Review, Clarence Hall Symposium volume, vol. 40, pp. 375–402.

Bennett, R.A., Wernicke, B.P., Niemi, N.A., Friedrich, A.M., Davis, J.L., 2003. Contemporary strain rates in the northern Basin and Range province from GPS data. Tectonics 22 (2), 1008. doi:10.1029/2001TC001355.

Brace, W.F., Bombalakis, E.G., 1963. A note on brittle crack growth in compression. Journal of Geophysical Research 68, 3709–3713.

Calais, E., d'Oreye, N., Albaric, J., Deschamps, A., Delvaux, D., Déverchère, J., Ebinger, C., Ferdinand, R.W., Kervyn, F., Macheyeki, A.S., Oyen, A., Perrot, J., Saria, E., Smets, B., Stamps, D.S., Wauthier, C., 2008. Strain accommodation by slow slip and dyking in a youthful continental rift, East Africa. Nature 456, 783–788.

Camp, V.E., Ross, M.E., 2004. Mantle dynamics and genesis of mafic magmatism in the intermountain Pacific Northwest. Journal of Geophysical Research 109. doi:10.1029/2003JB002838.

Christiansen, R.L., McKee, E.H., 1978. Late Cenozoic volcanic and tectonic evolution of the Great Basin and Columbia Intermontane regions. Geological Society of America Memoir 152, 283–311.

Christiansen, R.L., Yeats, R.S., 1992. Post-Laramide geology of the U.S. Cordilleran region. In: Burchfiel, B.C., Lipman, P.W., Zoback, M.L. (Eds.), The Cordilleran Orogen: Conterminous U.S.: Boulder, Colorado, Geological Society of America, The Geology of North America, G-3, pp. 261–406.

Christiansen, R.L., Foulger, G.R., Evans, J.R., 2002. Upper-mantle origin of the Yellowstone hotspot. Geological Society of America Bulletin 114, 1,245–1,256.

Cleary, J., Lange, I.M., Qamar, A.I., Krouse, H.R., 1981. Gravity, isotope, and geochemical study of the Alvord Valley geothermal area, Oregon. Summary, Geological Society of America Bulletin, Part I 92, 319–322.

Colgan, J.P., Dumitru, T.A., Miller, E.L., 2004. Diachroneity of Basin and Range extension and Yellowstone hotspot volcanism in northwestern Nevada. Geological Society of America Bulletin 32, 121–124.

Colgan, J.P., Shuster, D.L., Reiners, P.W., 2008. Two-phase Neogene extension in the northwestern Basin and Range recorded in a single thermochronology sample. Geology 36, 631–634.

Couch, R., Johnson, S., 1968. The Warner Valley earthquake sequence; May and June 1968. Oregon Geology 30, 191–204.

Crider, J.G., 2001. Oblique slip and the geometry of normal-fault linkage: mechanics and a case study from the Basin and Range in Oregon. Journal of Structural Geology 23, 1,997–2,009.

Densmore, A.L., Dawers, N.H., Gupta, S., Guidon, R., 2005. What sets topographic relief in extensional footwalls? Geological Society of America 33, 453–456.

Dilles, J.H., Gans, P.B., 1995. The chronology of Cenozoic volcanism and deformation in the Yerrington area, western Basin and Range and Walker Lane. Geological Society of America Bulletin 107, 474–486.

Donath, F.A., 1962. Analysis of basin–range structure, south-central Oregon. Geological Society of America Bulletin 73, 1–16.

Donath, F.A., Kuo, J.T., 1962. Seismic-refraction study of block faulting, south-central Oregon. Geological Society of America Bulletin 73, 429–434.

Duffield, W.A., McKee, E.H., 1986. Geochronology, structure, and basin–range tectonism of the Warner Range, northeastern California. Geological Society of America Bulletin 97, 142–146.

Duncan, R.A., Hogan, L.G., 1994. Radiometric dating of young MORB using the ^{40}Ar–^{39}Ar incremental heating method. Geophysical Research Letters 21, 1927–1930.

Duncan, R.A., Hooper, P.R., Rehacek, J., Marsh, J.S., Duncan, A.R., 1997. The timing and duration of the Karoo igneous event, southern Gondwana. Journal of Geophysical Research 102, 18127–18138.

Faulds, J.E., Henry, C.D., Hinz, N.H., 2005. Kinematics of the northern Walker Lane: an incipient transform fault along the Pacific-North American plate boundary. Geology 33, 505–508.

Fiebelkorn, R.B., Walker, G.W., MacLeod, N.S., McKee, E.H., Smith, J.G., 1983. Index to K–Ar determinations for the state of Oregon. Isochron West 37, 3–60.

Fosdick, J.C., Colgan, J.P., 2008. Miocene extension in the East Range, Nevada: a two-stage history of normal faulting in the northern Basin and Range. Geological Society of America Bulletin 120, 1198–1213.

Fuller, R.E., Waters, A.C., 1929. The nature and origin of the horst and graben structure of southern Oregon. Journal of Geology 37, 204–238.

Gilbert, G.K., 1928. Studies of Basin–Range Structure: U.S. Geological Survey Professional Paper, vol. 153. 92 pp.

Hamilton, W.B., 1989. Crustal geologic processes of the United States. In: Pakiser, L.C., Mooney, W.D. (Eds.), Geological Society of America Memoir, 172, pp. 743–781.

Hammond, W.C., Thatcher, W., 2005. Northwest Basin and Range tectonic deformation observed with the Global Positioning System, 1999–2003. Journal of Geophysical Research 110, B10405. doi:10.1029/2005JB003678.
Hart, W.K., Mertzman, S.A., 1982. K–Ar ages of basalts from southcentral and southeastern Oregon. Isochron-west 33, 23–26.
Hart, W.K., Aronson, J.L., Mertzman, S.A., 1984. Areal distribution and age of low-k, high-alumina olivine tholeitte magmatism in the northwestern Great Basin. Geological Society of America Bulletin 95, 186–195.
Hemphill-Haley, M.A., Page, W.D., Burke, R., Carver, G.A., 1989. Holocene activity of the Alvord fault, Steens Mountain, southeastern Oregon: final report to the U.S. Geological Survey under Grant No. 14-08-001-61333. 45 pp.
Henry, C.D., Perkins, M.E., 2001. Sierra Nevada-Basin and Range transition near Reno, Nevada; two stage development at 12 and 3 Ma. Geology 29, 719–722.
Hooper, P.R., Binger, G.B., Lees, K.R., 2002. Ages of the Steens and Columbia River flood basalts and their relationship to extension-related calc–alkalic volcanism in eastern Oregon. Geological Society of America Bulletin 114, 43–50.
Humphreys, E.D., 1994. Post-Laramide removal of the Farallon slab, western United States. Geology 23, 987–990.
Humphreys, E.D., Coblentz, D.D., 2007. North American dynamics and western U.S. tectonics. Reviews of Geophysics 45 30 pp.
Johnson, J.A., 1995. Geologic evolution of the Duck Creek Butte eruptive center, High Lava Plains, southeastern Oregon [M.S. Thesis]: Corvallis, Oregon, Oregon State University, 151 pp.
Johnson, J.A., Grunder, A.L., 2000. The making of intermediate composition magma in a bimodalsuite: Duck Butte Eruptive Center, Oregon, USA. Journal of Volcanology and Geothermal Research 95, 175–195.
Jordan, B.T., 2001. Basaltic volcanism and tectonics of the High Lava Plains, southeastern Oregon, [Ph.D. Thesis] Corvallis, Oregon, Oregon State University, 218 pp.
Jordan, B.T., Grunder, A.L., Duncan, R.A., Deino, A.L., 2004. Geochronology of Oregon High Lava Plains volcanism: mirror image of the Yellowstone hotspot? Journal of Geophysical Research 19 pp.
Khodayar, M., Einarsson, P., 2002. Strike–slip faulting, normal faulting, and lateral dike injections along a single fault: field example of the Gljúfurà fault near a Tertiary oblique rift-transform zone, Borgarfjörður, west Iceland. Journal of Geophysical Research (B5), 2103. doi:10.1029/2001JB000150.
Langer, V.W., 1991. Geology and petrologic evolution of silicic and intermediate volcanic rocks underneath Steens Mountain basalt, SE Oregon: Queen's University (CAN) M.S. thesis, 109 pp.
Langridge, R.M., Weldon, R.J., Pezzopane, S.K., Jellinek, A.M., 1996. Active faulting and tufa formation at Sawed Horn, central Oregon: a possible kinematic link between the Abert Rim and Viewpoint faults. Geological Society of America Abstracts with Programs 28 (5), 84.
Lawrence, R.D., 1976. Strike–slip faulting terminates the Basin and Range province in Oregon. Geologic Society of America Bulletin 87, 846–850.
Legge, P.W., 1988. The bimodal basalt–rhyolite association west of and adjacent to the Pueblo Mountains, southeastern Oregon [M.S. Thesis] Miami University of Ohio, Oxford, Ohio.
Ludwin, R.S., Weaver, C.S., Crosson, R.S., 1991. Seismicity of Washington and Oregon. In: Slemmons, D.B., Engdahl, E.R., Zoback, M.D., Blackwell, D.D. (Eds.), Neotectonics of North America: Boulder, Colorado: Geological Society of America, Decade Map, vol. 1, pp. 77–98.
Maloney, N.J., 1961. Geology of the Eastern Part Beaty Butte Four Quadrangle, Oregon, [M.S. Thesis], Oregon State University, Corvallis, Oregon, 88 pp.
Mankinen, E.A., Larson, E.E., Gromme, C.S., Prevot, M., Coe, R.S., 1987. The Steens Mountain (Oregon) geomagnetic polarity transition, its regional significance. Journal of Geophysical Research 92, 8057–8076.
Mathis, A.C., 1993. Geology and petrology of a 26-Ma trachybasalt to peralkaline rhyolite suite exposed at Hart Mountain, southern OR [M.S. thesis]: Corvallis, Oregon, Oregon State University, 141 pp.
McCaffrey, R., Qamar, A.I., King, R.W., Wells, R., Khazaradze, G., Williams, C.A., Stevens, C.W., Vollick, J.J., Zwick, P.C., 2007. Fault locking, block rotation and crustal deformation in the Pacific Northwest. Geophysical Journal International 169, 1315–1340.
Miller, E.L., Dumitru, T., Brown, R., Gans, P.B., 1999. Rapid Miocene slip on the Snake Range decollement. Geological Society of America Bulletin 111, 886–905.
Miller, M.M., Johnson, D.J., Dixon, T.H., Dokka, R.K., 2001. Refined kinematics of the Eastern California shear zone from GPS observations, 1993–1998. Journal of Geophysical Research 106, 2245–2263.
Minor, S.A., Plouff, D., Esparza, L.E., and Peters, T.J., 1987, Geologic map of the High Steens and Little Blitzen Gorge wilderness study areas, Harney County, Oregon: U.S. Geological Survey Miscellaneous Field Studies Map MF-1976, scale 1:24,000.
Murphy, R.T., Faulds, J.E., Hillemeyer, F.L., 2004. Evolution of Miocene extensional fault and fold systems and influence of magmatism in the northern Colorado River extensional corridor, Union Passarea, northwest Arizonea. Geological Society of America Abstracts with Programs 36 (4), 21.
Nakamura, K., Uyeda, S., 1980. Stress gradient in arc-back arc regions and plate subduction. Journal of Geophysical Research 85, 6419–6428.
Oldow, J.S., 2003. Active transtensional boundary zone between the western Great Basin and Sierra Nevada block, Western U.S. Cordillera. Geology 31, 1033–1036.
Pezzopane, S.K., Weldon, R.J., 1993. Tectonic role of active faulting in central Oregon. Tectonics 12, 1,140–1,169.
Rodgers, D.W., Ore, H.T., Bobo, R.T., McQuarrie, N., Zentner, N., 2002. Extension and Subsidence of the Eastern Snake River Plain, Idaho. In: Bill, Bonnichsen, White, C.M., Michael, McCurry (Eds.), Tectonic and Magmatic Evolution of the Snake River Plain Volcanic Province: Idaho Geol. Surv. Bull., vol. 30, pp. 5–33.
Rowley, P.D., 1998. Cenozoic transverse zones and igneous belts in the Great Basin, western United States: their tectonic and economic implications. In: Faulds, J.E., Stewart, J.H. (Eds.), Accommodation Zones and Transfer Zones: The regional Segmentation of the Basin and Range Province. Geological Society of America Special Paper, Boulder, Colorado, p. 323.
Sawlan, M.G., King, H.D., Plouff, D., Miller, M.S., 1995. Mineral resources of the Spaulding Wilderness study area, Lake and Harney Counties, Oregon. USGS Bulletin Report no. B1738-E. 18 pp.
Scarberry, K.C., 2007. Extension and volcanism: tectonic development of the northwestern margin of the Basin and Range province in southern Oregon [Ph. D. Thesis]: Corvallis, Oregon, Oregon State University, 168 pp.
Seedorff, E., 1991. Magmatism, extension, and ore deposits of Eocene to Holocene age in the Great Basin; mutual effects and preliminary proposed genetic relationships. In: Raines, G.L., Lisle, R.E., Schafer, R.W., Wilkinson, W.H. (Eds.), Geology and ore deposits of the Great Basin, Symposium Proceedings, pp. 133–178.
Sherrod, D.R., Smith, J.G., 2000. Geologic map of upper Eocene to Holocene volcanic and related rocks of the Cascade Range, Oregon. U.S. Geological Survey, Geologic Investigations Series-I-2569.
Sherrod, D.R., Griscom, A., Turner, R.L., Minor, S.A., Graham, D.E., Buehler, A.R., 1988. Mineral resources of the Sheepshead Mountains, Wildcat Canyon, and Table Mountain Wilderness Study Areas, Malheur and Harney counties, Oregon. U.S. Geological Survey Bulletin A1–A16.
Smith, G.A., Snee, L.W., Taylor, E.M., 1987. Stratigraphic, sedimentologic, and petrologic record of late Miocene subsidence of the central Oregon High Cascades. Geology 15, 389–392.
Streck, M.J., Grunder, 1995. Crystallization and welding variations in a widespread ignimbrite sheet: the Rattlesnake Tuff, eastern Oregon. Bulletin of Volcanology 57, 151–169.
Surpless, B.E., Stockli, D.F., Dumitru, T.A., Miller, E.L., Farley, K.A., 2002. Progressive westward encroachment of Basin and Range extension into the stable northern Sierra Nevada block. Tectonics 21 (1), 2-1–2-13.
Tentler, T., Mazzoli, S., 2005. Architecture of normal faults in the rift zone of central north Iceland. Journal of Structural Geology 27, 1721–1739.
Thatcher, W., Foulger, G.R., Julian, B.R., Svar, J.L., Quilty, E., Bawden, G.W., 1999. Present-day deformation across the Basin and Range Province, Western United States. Science 283, 1714–1718.
Trexler Jr., J.H., Cashman, P.H., Henry, C.D., Muntean, T.W., Schwartz, K., TenBrink, A., Faulds, J.E., Perlins, M., Kelly, T.S., 2000. Neogene basins in western Nevada document tectonic history of the Sierra Nevada – Basin and Range transition zone for the last 12 Ma. In: Lageson, D.R., Peters, S.G., Lahren, M.M. (Eds.), Great Basin and Sierra Nevada, 2. Boulder, Colorado, Geological Society of America Field Guide, pp. 97–116.
Trudgill, B., Cartwright, J., 1994. Relay-ramp forms and normal-fault linkages, Canyonlands National Park, Utah. Geological Society of America Bulletin 106, 1143–1157.
Walker, G.W., 1963. Reconnaissance Geologic map of the eastern half of the Klamath Falls (AMS) Quadrangle, Lake and Klamath Counties, Oregon. Mineral Investigations Field Studies Map MF-260, scale 1:250,000.
Walker, G.W., 1970. Cenozoic ash-flow tuffs of Oregon. Oregon Department of Geology and Mineral Industries 32 (6), 77–79 (Ore Bin).
Walker, G.W., MacLeod, N.S., 1991. Geologic map of Oregon. U.S. Geological Survey, Reston, VA.
Wells, R.E., 1980. Drake Peak—a structurally complex rhyolite center in southeastern Oregon. U.S. Geological Survey Professional Paper 1124-E. 16 pp.
Wells, R.E., Heller, P.H., 1988. The relative contribution of accretion, shear, and extension to Cenozoic tectonic rotation in the Pacific Northwest. Geological Society of America Bulletin 100, 325–338.
Wells, R.E., Weaver, C.S., Blakely, R.J., 1998. Fore arc migration in Cascadia and its neotectonic significance. Geology 26, 759–762.
Wernicke, B.P., 1992. Cenozoic extensional tectonics of the U.S. Cordillera. In: Burchfiel, B.C., et al. (Ed.), The Cordilleran orogen: Conterminous U.S. : Geology of North America, vol. G-3. Geological Society of America, Boulder, Colorado, pp. 553–581.
Wesnousky, S.G., 2005. The San Andreas and Walker Lane fault systems, western North America: transpression, transtension, cumulative slip and the structural evolution of a major transform plate boundary. Journal of Structural Geology 27, 1505–1512.
Zandt, G., Humphreys, E., 2008. Toroidal mantle flow through the western U.S. slab window. Geology 36, 295–298.
Zoback, M.L., 1989. State of stress and modern deformation of the Northern Basin and Range Province. Journal of Geophysical Research 94, 7105–7128.